ISTANBUL TECHNICAL UNIVERSITY ★ GRADUATE SCHOOL

EFFECT OF RF MAGNETRON SPUTTERING PARAMETERS ON ELECTROCHROMIC PROPERTIES OF NICKEL OXIDE THIN FILMS

M.Sc. THESIS

Ece KURT

Department of Physics Engineering

Physics Engineering Programme

JULY 2021

ISTANBUL TECHNICAL UNIVERSITY ★ GRADUATE SCHOOL

EFFECT OF RF MAGNETRON SPUTTERING PARAMETERS ON ELECTROCHROMIC PROPERTIES OF NICKEL OXIDE THIN FILMS

M.Sc. THESIS

Ece KURT
(5091810)

Department of Physics Engineering

Physics Engineering Programme

Thesis Advisor: Prof. Dr. Esra ZAYİM
Co-Advisor: Assoc. Prof. Dr. Mustafa ALTUN

JULY 2021

ISTANBUL TEKNİK ÜNİVERSİTESİ ★ LİSANSÜSTÜ EĞİTİM ENSTİTÜSÜ

RF MAGNETRON SIÇRATMA PARAMETRELERİNİN NİKEL OKSİT İNCE FİLMLERİN ELEKTROKROMİK ÖZELLİKLERİNE ETKİSİ

YÜKSEK LİSANS TEZİ

Ece KURT
(509181107)

Fizik Mühendisliği Anabilim Dalı

Fizik Mühendisliği Programı

Tez Danışmanı: Prof. Dr. Esra ZAYİM
Eş Danışman: Doç. Dr. Mustafa ALTUN

TEMMUZ 2021

Ece KURT, a M.Sc. student of ITU İTU Graduate School student ID 509181107, successfully defended the thesis entitled "EFFECT OF RF MAGNETRON SPUTTERING PARAMETERS ON ELECTROCHROMIC PROPERTIES OF NICKEL OXIDE THIN FILMS", which she prepared after fulfilling the requirements specified in the associated legislations, before the jury whose signatures are below.

Thesis Advisor :	**Prof. Dr. Esra ZAYIM** Istanbul Technical University	.....
Co-advisor :	**Assoc. Prof. Dr. Mustafa ALTUN** Istanbul Technical University	.....
Jury Members :	**Assoc. Prof. Dr. Zuhal ER** Istanbul Technical University	.....
	Asst. Dr. Tolga TAVŞANOĞLU Mugla Sitki Kocman University	.....
	Prof. Dr. Ayşegül UYGUN ÖKSÜZ Suleyman Demirel University	.....

Date of Submission : 10 June 2021
Date of Defense : 12 July 2021

To science,

FOREWORD

I would like to present my gratitude to my director of studies, Prof. Dr. Esra ZAYIM whose deepest knowledge, sharing, and helped not only my studies and also helped to establish my working discipline and world-view. I would like to thank my co-advisor Assoc. Prof. Dr. Mustafa ALTUN for all of his guidance through this process; your discussion, ideas, and feedback have been absolutely invaluable.

I would like to express my gratitude to Dr. Seniz TÜRKÜZ who gave me an opportunity to use all the facilities of Sisecam Science Technology and Design Center, Vacuum Coating Department.

I would particularly like to single out my supervisor at Sisecam, Dr. Öcal TUNA. I want to thank you for your patient support and all of the opportunities I was given to further my research.

I want to thank Duygu NUHOĞLU for the effective collaboration on my thesis studies and endless friendship. I would like to thank the following people, Fatma Beyza YEDİKARDEŞ and Rümeysa SALCI for their endless friendship and support.

July 2021

Ece KURT

(Physics Engineer)

TABLE OF CONTENTS

Page

ABBREVIATIONS

EC : Electrochromic
ECD : Electrochromic Device
TMO : Transition Metal Oxide
TCO : Transparent Conducting Oxide
CV : Cyclic Voltammetry
CA : Chronoamperometry
CE : Coloration Efficiency
OD : Optical Density
Qin : Inserted Charge
Qout : Extracted Charge
XRD : X-Ray Diffraction
XRR : X-Ray Reflection
AFM : Atomic Force Microscopy
FEGSEM : Field Emission Gun Scanning Electron Microscopy
ITO : Indium Tin Oxide
WO_3 : Tungsten Trioxide
NiO : Nickel Oxide
PC : Propylene Carbonate
Ag/AgCl : Silver/Silver Chloride
Pt : Platinum

SYMBOLS

n	**:** Refractive Index
λ	**:** Wavelength (nm)
W	**:** Watt
V	**:** Voltage
q	**:** Charge
t	**:** Time
mTorr	**:** Milli Torr
mC	**:** Milli Coulomb
mA	**:** Milli Amper
nm	**:** Nanometer (10^{-9} m)
Å	**:** Angstrom (10^{-10} m)

LIST OF TABLES

Page

LIST OF FIGURES

Page

EFFECTS OF RF MAGNETRON SPUTTERING PARAMETERS ON ELECTROCHROMIC PROPERTIES OF NICKEL OXIDE THIN FILMS

SUMMARY

Since a high proportion of the energy lost in architectural structures is due to windows, developments in the smart glass industry have accelerated in recent years. The reason why electrochromic glasses are the most preferred smart glass applications is that there is a reversible and sustainable change in optical properties with the electric field created by a small applied voltage. These glasses have a structure consisting of layers with different properties. By optimizing the layers with different properties that build up smart glasses, features such as optical modulation in the visible region, coloring efficiency and long-term durability, which are important in evaluating smart glass performance, can be improved. One of the layers, anodic electrochromic thin film, has been studied in detail by researchers for many years due to its ion storage and optical modulation improvement properties in smart glasses. One of the most commonly used materials for this layer is nickel oxide thin films. RF magnetron sputtering technique is a preferred method in the production of electrochromic devices due to its advantages such as commercialization potential, widespread use and ease of change in sputtering parameters. The significant effect of surface porosity on the electrochromic properties of transition metal oxides has been studied in the literature. However, the effect of surface porosity on electrochromic properties of nickel oxide thin films deposited by RF sputtering technique, depending on sputtering parameters, has not been studied in detail.

In this thesis, the optimization of nickel oxide thin films deposited on ITO/glass substrates was performed by RF magnetron sputtering method, depending on sputtering parameters. For this purpose, thin films were prepared at different oxygen partial pressures, RF sputtering powers and pressures. Depending on the variations in RF sputtering parameters, the changes in their structural, morphological, optical and electrochromic properties were examined in detail. The structural properties of the nickel oxide thin film were investigated by x-ray diffraction (XRD). X-ray reflectometry (XRR) was used to determine the density of the films. The surface morphologies of the films were investigated by atomic force microscopy (AFM) and scanning electron microscopy (SEM), and their optical properties were investigated by ellipsometry and spectrophotometry. Surface porosities of nickel oxide thin films deposited on transparent conductive oxide substrates under different sputtering conditions were determined. The electrochemical properties of the films were investigated in detail by cyclic voltammetry (CV) and chronoamperometry (CA).

In the study, oxygen partial pressure, sputtering power and pressure, which are RF magnetron sputtering parameters, were changed in control. The thickness of the thin films deposited throughout the study was kept constant at around 150±30 nm. All experiments were performed at room temperature and at a fixed target substrate distance. In order to examine the effect of oxygen partial pressure, that is, the reactive oxygen gas content (O_2/O_2+Ar) in the plasma, on the electrochromic properties of nickel oxide thin films, coatings were made with an oxygen content of 50, 60, 75,90%. The coatings were performed at 60W constant sputtering power and 13mTorr constant

working pressure. As a result of detailed characterizations, it was determined that the films coated with 90% oxygen content exhibited the best electrochromic properties. After deciding on the amount of oxygen, coatings with powers of 60, 75, 90, 105W were made in order to examine the effect of sputtering power on the electrochromic properties of nickel oxide thin films. To examine the effect of sputtering power, the oxygen content was kept constant at 90% and the sputtering pressure at 13mTorr. As a result of the characterizations, it was determined that the film coated with 90W sputtering power exhibited the best electrochromic properties. After deciding on the splash power, coatings were made at 13, 15, 17 and 25 mTorr in order to examine the effect of the sputtering pressure. As a result of the characterizations, it was determined that the film coated with 13 mTorr sputtering pressure exhibited the best electrochromic performance.

Although nickel oxide is the most studied material among other anodic electrochromic materials, this thesis has contributed to the literature in determining the effect of RF magnetron sputtering parameters on the electrochromic properties of nickel oxide thin films due to surface porosity.

RF MAGNETERON SIÇRATMA PARAMETRELERİNİN NİKEL OKSİT İNCE FİLMLERİN ELEKTROKROMİK ÖZELLİKLERİNE ETKİSİ

ÖZET

Mimari yapılarda kaybedilen enerjinin büyük bir kısmı camlardan kaynaklandığı için akıllı cam sektöründeki gelişmeler son yıllarda hız kazanmıştır. Akıllı camlar sıcaklık, potansiyel fark ve elektromanyetik radyasyon gibi dış uyaranların etkisi altında optik özelliklerini değiştiren malzemelerden oluşmaktadır.

Elektrokromik camların en çok tercih edilen akıllı cam uygulamaları olmasının nedeni, uygulanan küçük bir voltajın oluşturduğu elektrik alanı ile optik özelliklerde tersinir ve sürdürülebilir bir değişim olmasıdır.

Elektrokromik akıllı camlar şeffaf iletken oksit katman, elektrokromik katman ve iyon iletken katman olmak üzere birkaç ince film katmanından oluşmaktadır. Günümüzde farklı konfigürasyonlara sahip akıllı camlar bulunsada, en genel haliyle elektrokromik akıllı cam bu ince film katmanlarını içeren yedi katmandan oluşmaktadır. Şeffaf iletken oksit katman, akıllı camın çalışması için gerekli olan elektrik potansiyelinin uygulanabileceği iletken katmandır. Elektrokromik akıllı camlar, şeffaf iletken katman üzerine biriktirilmiş, birbirine zıt yükseltgenme/indirgenme tepkimeleri ile optik özelliklerini değiştiren iki elektrokromik ince filmin, organik ya da inorganik malzeme içerikli bir iyon iletken katman olan elektrolit ile lamine edilerek oluşturulmaktadır.

Elektrokromik katmanlar cihazın optik özelliklerinde değişime neden olan katmanlardır. Bu katmanların yapısal, morfolojik, optik ve elektrokimyasal özelliklerinin optimizasyonu ile akıllı cam performansının değerlendirilmesinde önemli olan görünür bölgedeki optik modülasyon, renklendirme verimliliği ve uzun süreli dayanıklılık gibi özellikler iyileştirilebilir. Elektrokromik katmanlar anodik ve katodik olmak üzere iki ayrı grupta incelenebilirler.

Akıllı cam katmanlarından biri olan anodik elektrokromik ince film, akıllı camlarda iyon depolama ve optik modülasyon iyileştirme özellikleri nedeniyle uzun yıllardır araştırmacılar tarafından detaylı olarak incelenmektedir. Bu katman için en yaygın olarak kullanılan malzemelerden biri nikel oksit ince filmlerdir. Bu ince filmlerin üretimi için fiziksel ve kimyasal olmak üzere farklı kaplama yöntemleri kullanılmaktadır. Ancak, bu kaplama türleri arasından RF magnetron sıçratma tekniği, ticarileşme potansiyeli, yaygın kullanımı ve sıçratma parametrelerinin kolay değiştirilebilirliği gibi avantajlarından dolayı elektrokromik aygıtların üretiminde tercih edilen bir yöntemdir. RF magnetron sıçratma tekniğinde sıçratma parametrelerinin değişimi, ince filmlerin özelliklerini etkilemektedir.

Yüzey porozitesinin geçiş metal oksitlerinden meydana gelen ince filmlerin elektrokromik özellikleri üzerindeki önemli etkisi literatürde incelenmiştir. Ancak RF magnetron sıçratma tekniği ile biriktirilen nikel oksit ince filmlerin sıçratma parametrelerine bağlı olarak yüzey porozitesinin, elektrokromik özelliklerine etkisi detaylı olarak çalışılmamıştır.

Bu tez çalışmasında, indiyum kalay oksit (ITO)/cam altlıklar üzerine biriktirilen nikel oksit ince filmlerinin RF magnetron sıçratma yöntemi ile sıçratma parametrelerine

bağlı olarak optimizasyonu gerçekleştirilmiştir. Bu amaçla farklı oksijen kısmi basınçlarında, RF sıçratma güçlerinde ve basınçlarında ince filmler hazırlanmıştır.

Değişen RF sıçratma parametrelerine bağlı olarak NiO ince filmlerin yapısal, morfolojik, optik ve elektrokromik özelliklerindeki değişimler detaylı olarak incelenmiştir. Nikel oksit ince filmin yapısal özellikleri x-ışını kırınımı (XRD) ile incelenmiştir. Filmlerin yoğunluğunu bulmak için x-ışını reflektometrisi (XRR) kullanılmıştır. Filmlerin yüzey morfolojileri atomik kuvvet mikroskobu (AFM) ve taramalı elektron mikroskobu (SEM) ile, optik özellikleri ise elipsometri ve spektrofotometri ile araştırılmıştır. Farklı sıçratma koşullarında saydam iletken oksit altlıklar üzerine biriktirilen nikel oksit ince filmlerin, yüzey poroziteleri belirlenmiştir. Filmlerin elektrokimyasal özellikleri çevrimsel voltametri (CV) ve kronoamperometri (CA) ile detaylı olarak incelenmiştir.

Çalışmada, RF magnetron sıçratma parametreleri olan oksijen kısmi basıncı, sıçratma gücü ve sıçratma basıncı kontrollü bir şekilde değiştirilmiştir. Çalışma boyunca kaplanan ince filmlerin kalınlıkları 150±30 nm civarında sabit tutulmuştur. Tüm deneyler oda sıcaklığında gerçekleştirilmiştir. Kaplamalar yapılırken hedef altlık mesafesi sabit tutulmuştur.

Yapılan ön deneylerde, oksijen kısmi basıncı %0 ile %100 aralığında değiştirilerek sputter kaplama oranının değişimi incelenmiştir. Bu değişim ile tamamen oksitlenmiş nikel oksit ince filmler kaplamak için oksijen kısmi basınç aralığı %50 ile %90 olarak belirlenmiştir.

İlk deney setinde, oksijen kısmi basıncının yani plazma içine katılan reaktif oksijen gazı içeriğinin (O_2/O_2+Ar) nikel oksit ince filmlerin elektrokromik özelliklerine etkisi incelenmiştir. Oksijen içeriği %50, 60, 75 ,90 olacak şekilde kaplamalar yapılmıştır. Kaplamalar 60 W sabit sıçratma gücü ve 13 mTorr sabit çalışma basıncında gerçekleştirilmiştir. Kaplanan nikel oksit ince filmler için yapılan detaylı karakterizasyonlar sonucunda, %90 oksijen içeriği ile kaplanan filmlerin en iyi elektrokromik özelliği sergiledikleri tespit edilmiştir.

En iyi elektrokromik özelliklere sahip nikel oksit ince filmlerin elde edildiği oksijen miktarına karar verildikten sonra, sıçratma gücünün nikel oksit ince filmlerin elektrokromik özelliklerine etkisini incelemek amacıyla 60, 75, 90, 105 W güçlerinde kaplamalar yapılmıştır. Sıçratma gücünün etkisini incelemek için oksijen içeriği %90 ve sıçratma basıncı 13 mTorr olarak sabit tutulmuştur. Farklı sıçratma güçlerinde kaplanan nikel oksit ince filmler için yapılan karakterizasyonlar sonucunda 90 W sıçratma gücü ile kaplanan filmin en iyi elektrokromik özellikleri sergilediği belirlenmiştir.

En iyi elektrokromik özelliklere sahip nikel oksit ince filmlerin elde edildiği sıçratma gücüne karar verildikten sonra, sıçratma basıncının nikel oksit ince filmlerin elektrokromik özelliklerine etkisini incelemek amacıyla 13, 15, 17 ve 25 mTorr'da kaplamalar yapılmıştır. Oksijen içeriği %90 ve sıçratma gücü 90 W olarak sabit tutulmuştur. Farklı sıçratma basınçlarında kaplanan nikel oksit ince filmler için yapılan karakterizasyonlar sonucunda 13 mTorr sıçratma basıncı ile kaplanan filmin en iyi elektrokromik performans sergilediği tespit edilmiştir.

Nikel oksit diğer anodik elektrokromik malzemeler arasında en çok çalışılan malzeme olmasına rağmen bu tez çalışması, RF magnetron sıçratma parametrelerinin nikel oksit

ince filmlerin yüzey porozitesine bağlı elektrokromik özellikleri üzerindeki etkisini belirleme konusunda literatüre katkı sağlamıştır.

1. INTRODUCTION

In recent years, concern about energy resource depletion issue makes the world face off a big energy crisis. The energy crisis is due to the predictable end of the oil, gas and coal cycle. Therefore, the trend towards natural resources such as wind, sun, and wave power, which can be used for new energy sources, has increased. Accordingly, research and development projects have been conducted on developing and searching for energy consumption methods. The buildings use 30 to 40% of primary energy and 25 to 35% of energy in buildings is wasted because of windows. For this reason, the design and properties of the transparent elements that form the envelope of the building are being developed hereby up to 17 % of the energy can be saved by windows [1]. Many researchers focus on smart glass doors and windows to apply electrochromic technology, as they provide huge energy savings and indoor temperature control in buildings. Electrochromic smart windows have the ability to sustain reversible optical changes under the application of a small voltage with created an external electric field. Electrochromic smart windows (devices) have a multilayer sandwich structure in which electrochromic thin films are used [2]. Therefore electrochromic thin films used in an electrochromic device attract much interest in forthcoming technology [3] [4]. Transition metal oxides are in the most preferred material class for electrochromic applications, as they allow to control of various optical parameters such as absorption, transmittance, and reflection, and basic optical properties such as refractive index (n) and extinction coefficient (k) [5]. Transition metal oxides such as titanium (Ti), vanadium (V), molybdenum (Mo), tungsten (W), and nickel (Ni) oxides are widely studied for their electrochromic behavior [6][7][8]. For the design of the electrochromic device, the structure in which the ion conductive layer in the center, the cathodic electrochromic tungsten oxide film as the electrochromic layer, and the anodic electrochromic nickel oxide film as the ion-storing layer is combined, has recently received special attention [9][10][11]. The combination of these two electrochromic materials in the electrochromic device structure is suitable because of the compatibility of their electrochemical potentials. The counter electrode (anodic electrochromic layer) layer is so important for providing the amount of ions required

to color electrochromic layer and increasing the optical modulation of electrochromic devices. For the counter electrode layer to be used for the electrochromic device, nickel oxide has been studied for many years because of its high electrochromic efficiency, wide optical modulation, high cyclic reversibility, and suitability for large-scale applications [12][13]. NiO electrochromic thin films were coated with many coating techniques like sol-gel [14], electrodeposition [15], chemical vapor deposition [16] and sputtering [17], and their electrochromic properties were investigated. Compared to these methods, magnetron sputtering, with its ease of parameters control and large scale uniform thin film production of NiO thin film, is one of the most promising techniques. By optimizing the RF magnetron sputtering parameters, superior performance can be achieved by improving optical modulation, optical density, charge capacity, film density and porosity, which are the most important features in evaluating the electrochromic performance of the electrochromic films [18] [19] [20].

2. ELECTROCHROMISM

Chromism has been studied at the academic and industrial levels since the 1900s. The chromogenic effect refers to the reversible modification of optical characteristics of a material as a function of external stimulus such as optical, thermal, electrical or among others[21]. Such reversible optical properties can be classified in different categories such as, photochromic [22] [23], thermochromic [24][25][26], electrochromic [27][28], which vary in their optical properties depending on the energy source and stimulus. The external stimulus can consist of electromagnetic radiation, electric current, heat, or among others. Photochromic materials alter their color upon exposure the electromagnetic radiation as external stimuli. The infrared (IR) and ultraviolet (UV) light can significantly affect the optical properties of photochromic materials. Due to the modification in the compound structure of the material, the absorption change occurs in visible region (400-750 nm) and color changes [29]. Different materials may respond with their own characteristic transmission spectra that transform in the presence of light variations. Tungsten oxide (WO_3) [30], molybdenum oxide (MoO_3) [31], zinc oxide (ZnO) [32], titanium oxide (TiO_2) [33] are well-known oxides exhibiting photochromic properties toward UV exposure. Photochromic materials can be used in displays, smart windows, among others devices and other photosensitive devices. Also, optical/electronic devices, drug delivery systems, sensors, etc. smart photosensitive devices have emerged as new opportunities in the use of photochromic materials [34] [35] [36].

Thermochromic materials can change their color in response to a variation in temperature reversibly. Quite a few organic and inorganic materials are known to have a very efficient thermochromic effect. Some applications have been developed using these materials in the fields of display[37], sensor[38], health technologies[39] and textile products [40]. Among organic materials, polydiacetylenes[41], poly(3-hexylthiophene)[42], and others exhibit thermochromism at various temperature ranges. Polymers such as silanes and siloxanes also exhibit thermochromic conversion [43][44]. Many transition metal (Ti, V, Nb, etc.) oxides show thermochromic

transformation over a wide temperature range [45] [46]. VO_2 has become the object of numerous scientific research and industrial applications as it exhibits a thermochromic phase transition at the temperature closest to room temperature (68ºC). Electrochromic materials reversibly vary in their optical properties, such as reflection, transmittance, and absorption, in response to the application of a small voltage. Electrochromism is more advantageous than other chromogenic behavior as it has ability to reversibly change optical properties independently of external conditions, rapidly change the degree of coloring/decolorization, and retain it without additional power support [47]. The multilayer sandwich structure in which electrochromic materials are used to change optical properties is called an electrochromic device (ECD). They have been finding several applications like automotive rearview mirrors, electronic papers [48], display systems [49], smart windows [50].

Electrochromic devices can be categorized as inorganic metal oxides, organic polymers, and hybrid materials. Metal oxides such as WO_3 [51], NiO [52], MoO_3 [53], and V_2O_5 [54], etc. have been used as an inorganic EC material where small ions (Li^+, H^+; K^+) enter the crystal matrix and cause color changes by an applied low voltage. Due to their low voltage operation, metal oxide based electrochromic devices operate efficiently with electrical energy consumption and show high optical contrast [55]. Organic molecules and conjugated polymers are used in electrochromic devices due to their different UV-vis absorption spectrum behavior depending on the redox state. Organic molecules and conjugated polymers such as poly-pyrrole (PPy) [56], polythiophenes (PThs) [57], and polyaniline (PANI) [58], poly(3,4-ethylene dioxythiophene) (PEDOT) [59] are the most commonly used materials in electrochromic polymer devices. Electrochromic polymers (ECPs) are used in both transmissive and reflective electrochromic devices due to their fast response times, high optical contrasts, low-cost production, and long-term optical stability properties. However, the synthesis and purification of organic EC materials limit their large-scale application due to their involvement in multi-step procedures, poor conductivity, and stability.

2.1 Electrochromic Device

The electrochromic smart window, ie the electrochromic device (ECD), consists of thin-film layers in a sandwich structure, consisting of two transparent conductive

oxides, two electrochromic layers, and an ion conductive layer. The structure of ECD is s chematized in figure 2.1. The electrochromic films which are counter electrode layer and electrochromic layer have opposite coloring behavior.

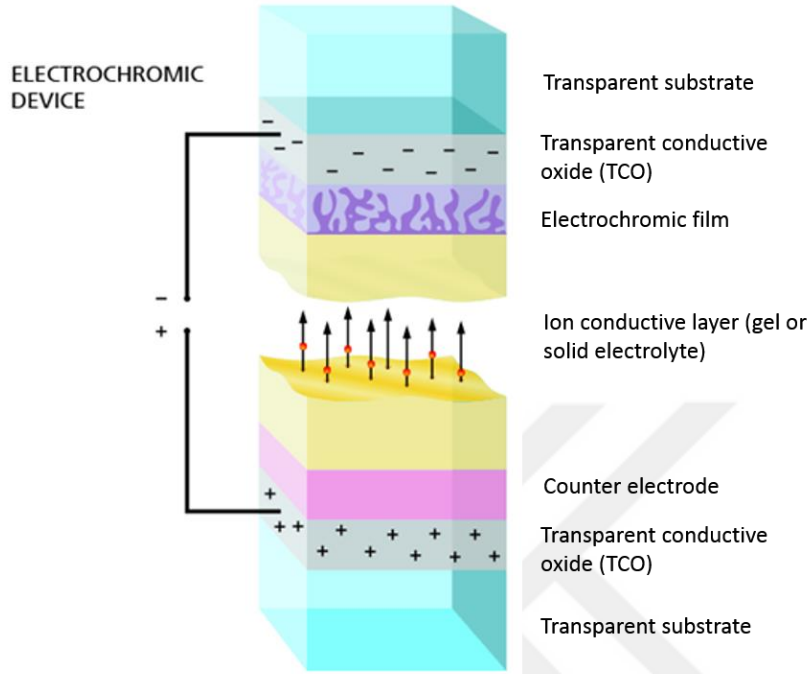

Figure 2.1: Schematic view of the electrochromic device structure [51].

In the initial state, the ions in the ion storage layer and the electrons in the outer circuit move towards the electrochromic layer due to the electric field created as a result of the electrical potential applied to the transparent conductive oxide layers as shown in the figure 2.1.

The electrochromic layer diffused by the ions becomes colored. For reverse optical exchange, the polarity of the electric potential is reversed and the ions are reversed in the opposite direction. With the reverse applied electrical potential to the transparent conductive oxide layers, ions and electrons move towards the counter electrode layer and both electrochromic and counter electrode layers become transparent. The transparency of the electrochromic device will be changed due to these process. Change in optical transmittance of the device is not limited to visible color changes, it can show optical modulation in the near infrared [60] and microwave regions [61]. Layer properties and materials used in the literature will be explained in the following sections.

2.1.1 Transparent substrate

Depending on the area of use of the electrochromic device polyester, polyethylene (PET), or glass can be used as a transparent substrate. PET substrates are used in areas such as robotic skin, biosensors, and supercapacitors in flexible wearable device technology, which is one of the areas of use of electrochromic devices, due to their flexible, shapeable structure, and high transparency [62] [63]. Glass substrates are used for smart window applications of electrochromic devices due to their high optical transmittance.

2.1.2 Transparent conductive oxide layer

An electrochromic device consists of two transparent conductive oxide (TCO) layers coated on transparent substrates. TCO is used to apply an electric field to the ECD to transport the charges to the electrochromic layers. The optical requirement for these layers is that they are highly transparent in the respective spectral region and are optically invariable in colored or bleached state of the system. It is expected that these layers have low resistivity (5-20 Ω/cm) for uniform application of the electric field, corresponding to the uniform coloration, to the ECD.

As it is known from the literature, indium-doped tin oxide (ITO) [64], gallium-doped zinc-oxide (GZO) [65], fluorine-tin oxide (FTO) [66], and aluminium-doped zinc oxide (AZO) [67] are the most commonly used transparent conductive oxides in ECDs, as they compensate these optical and electrical requirements very well.

Besides TCOs, some other transparent conductive electrode materials have been investigated to provide electrical conductivity, which serves to generate electric field in ECD. The use of other transparent electrodes enabled the device to improve other features such as electrical consumption, response time, and optical contrast.

Carbon materials such as carbon nanotubes (CNTs) [68] and graphene [69] have been used as alternatives to TCOs due to their intrinsic electrochemical stability and good electrical conductivity. In addition to carbon materials, PEDOT:PSS and silver grid transparent conductors are among the electrode materials being investigated to enable TCO-free ECD fabrications [70].

2.1.3 Counter electrode and electrochromic layer

The counter electrode layer plays important role in providing amount of ions required for coloring the electrochromic layer. As this counter electrode layer is also an ion storage layer, it is expected to have a high charge capacity that will be sufficient for the EC layer to be colored efficiently. In this case, it supports the change in the coloration level of the device. In some cases, this layer does not change its transparency when the device operates and only provides ion storage. This layer must work by undergoing redox reactions in harmony with the electrochromic layer. The well-known inorganic counter electrode layers in literature are nickel oxide (NiO) [71], iridium oxide (IrO_x) [72], rhodium oxide (Rh_2O_5) [73], and cobalt oxide [73]. To enhance the best performance for ECD, the properties of this layer should be optimized such as its structural, optical, electrical properties, and thickness. The electrochromic layer has opposite behavior with respect to the counter electrode layer . The well-known inorganic cathodic electrochromic layers in literature are tungsten oxide (WO_3) [74], molybdenum oxide (MoO_x), titanium oxide (TiO_2) [75], and niobium oxide (Nb_2O_5) [76].

2.1.4 Ion conductive layer

The ion conductive layer (electrolyte) separates the electrochromic and the counter electrode layer. Under the influence of the applied electric field, this layer should be ion conductive but electronically an insulator. The optical requirement for this film is that the electrochromic device is stable in optical transmittance in the colored and colorless states and highly transparent in the spectral region of interest. The ion conductive layer can be in gel or solid form. Depending on the activation of electrochromic layers, that is, the material of the ion conductive layer is chosen according to the type of ion (H^+, Li^+, etc.) chosen for the appropriate redox reaction. There are two types of electrolytes in an ECD, organic (polymer) and inorganic. In literature, the most used organic electrolytes are nafion [77], poly(acrylic acid) [78], poly(methylmethacrylate) – PMMA [79], and poly(ethylene oxide) - PEO[80] in the form of semi-solid film. The well-known inorganic electrolytes are $LiNbO_3$ [81], ZrO_2 [82], Ta_2O_5 [83], Sb_2O_5 [84] in the form of solid film. On the other hand, liquid electrolytes are used to determine the electrochromic performance of an

electrochromic thin film such as lithium perchlorate in propylene carbonate ($LiClO_4$-PC) anhydrous electrolyte, or potassium hydroxide (KOH) aqueous electrolyte [85].

2.2 Electrochromic Performance Parameters

In this section, the most important parameters to determine electrochromic performances of an electrochromic thin film were explained. The optical property of an ECD is one of the most important parts to determine its performance. The optical state in the spectral region of interest is called bleached or colored. By creating an electric field on ECD, the device will be in one of these states. The colored state means that the ECD has the lowest optical transmittance and the bleached state means that the ECD has the highest optical transmittance. The transmittance of electrochromic devices in bleached and colored states can be given as T_b and T_c abbreviations, respectively.

2.2.1 Optical modulation

The transmittance difference between colored and bleached states at a constant wavelength (λ) in spectral region of interest is called as optical modulation (ΔT) and calculated with the following equation 2.1.

$$\Delta T = T_b(\lambda) - T_c(\lambda) \quad (2.1)$$

The optical modulation is expected to be high.

2.2.2 Coloration efficiency (η)

Coloration efficiency (CE) is one of the most important parameter for selecting an electrochromic material and is defined as the change in optical density (ΔOD) per unit inserted charge (Q_{in}). CE is calculated with the equation 2.2.

$$CE = \frac{\Delta OD}{Q_{in}} \quad (2.2)$$

The optical density (ΔOD) is the logarithm of the transmittance differences between the colored and bleached state at a constant wavelength. ΔOD is calculated with the equation 2.3.

$$\Delta OD = \ln \frac{T_b(\lambda)}{T_c(\lambda)} \quad (2.3)$$

2.2.3 Response time

Response time is the time it takes to transform the coloration states occurring in an electrochromic device to each other. Typically, these response times are not the same for both cases. While the response times are desired to be short in some applications, it is desired to be long in others. For example, the electrochromic device to be used at home or workplace is desired to have a long response time, because sudden color changes can easily distract people. However, on the display screens, this period should be very short, so screen changes will be performed quickly. The determination of response time will be given in next sections.

2.3 Electrochromism in Nickel Oxide

Nanostructured transition metal oxides have gained great interest for electrochemical applications because that the physical properties of these materials easily change through stoichiometry and pressure. Especially oxides of various transition metals (tungsten, nickel, palladium, titanium, vanadium, cerium) exhibit electrochromic properties. The reason for the color changes occurring in the visible region in these materials is the charge transfer between the valence (intervalence) of the metal oxides. Among the other transition metal oxide, nickel oxide (NiO) has shown good electrochemical performance. Due to the optical, magnetic, electronic, and mechanical properties of NiO, it has gained attention to be used as smart windows, supercapacitor, electrode, and electrochromic device [86]. In transition metals, valence electrons are found in more than one shell, and owing to these electrons they combine with other elements. This is why they exhibit several common oxidation states. Nickel, which has different oxidation levels such as 0, +1, +2, +3, +4, is usually valued at +2 in its oxidized state. The electronic arrangement is [Ar] $4s^2 3d^8$. NiO is a wide band stable p-type semiconductor with a band gap ranging from 3.6-4.0 eV [87]. Stoichiometric Ni oxide has a cubic rock salt structure with octahedral Ni^{2+} and O^{2-} sites. The crystal structure of NiO is as shown in figure 2.2.

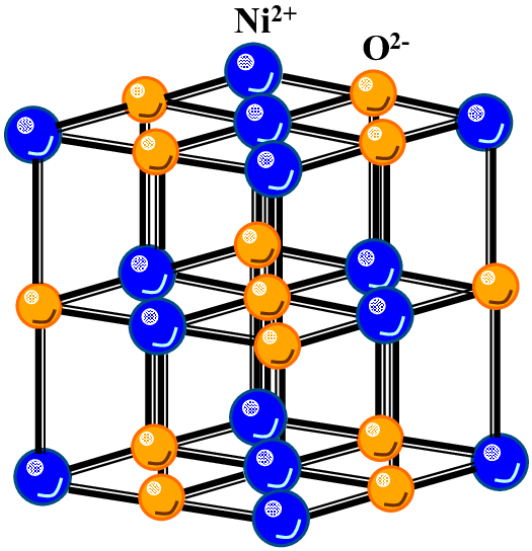

Figure 2.2: Crystal structure of NiO.

If Ni:O ratio is 1:1, nickel oxide has non-stoichiometric crystal structure. In nickel oxide, this non-stoichiometry is accompanied by a color change, with the stoichiometrically correct NiO being green and the non-stoichiometric NiO being brown [88]. Ni vacancies are defects in non-stoichiometric NiO [89] and Ni^{3+} formation is connected with these vacancies. The valence band consists of almost completely hybridized Ni 3d and O 2p states. The conduction band contains a mixture of O 2p states and empty Ni 3d states. Electrochromic coloration in NiO thin films occurs by removing and adding 3d electrons to the valence band. This situation occurs without affecting the Ni-O bond. Optical absorption in the colored/bleached states is related to charge transfer between Ni^{2+} and Ni^{3+} sites [52] [87].

The ions generally preferred for the electrochromic device to change color by charged (ion) intercalation are proton (H^+) and lithium (Li^+) due to their smaller size and easy intercalation [88] [90]. Electrochromic NiO has been done using aqueous electrolytes, especially potassium hydroxide (KOH). In this case, proton insertion/extraction occurs. However, a self-discharge phenomenon associated with the dissolution of partially oxidized phases for the KOH electrolyte has been reported to lead to a gradual decrease in poor stability [91]. In addition, the insertion of Li^+ ions in nickel oxide is faster than OH^- (KOH electrolyte) ions due to its smaller size [92]. In this study, non-aqueous lithium perchlorate in propylene carbonate ($LiClO_4$-PC) electrolyte was used because of both the degradation of the KOH solution and the best performance of the WO_3 material, which is mostly used in smart glass applications, in the electrolyte containing

Li-ions. A proposed two step intercalation mechanism has been explained that how NiO_x reacts to Li^+ by Passerini et al. in literature. Initially, the added Li^+ ions cause volume changes and strain in NiO_x. These changes are the reason of an irreversible modification of the NiO_x structure. This means that in the first step, the initially combined Li^+ ions activate the NiO_x structure, creating Li_yNiO_x. This activation procedure can be shown as following reaction (2.4).

$$NiO_x + yLi^+ + ye^+ \rightarrow Li_yNiO_x \quad (activation\ procedure) \tag{2.4}$$

In the second step, a reversible intercalation/deintercalation of charges process occures which is the associated with the electrochromic effect. This step can be shown as following reaction (2.5)

$$\underset{colored\ (brownish)}{Li_yNiO_x} \leftrightarrow \underset{bleached}{Li_{y-z}NiO_x} + zLi^+ + ze^- \tag{2.5}$$

Accordingly, the new structure is not NiO_x but electrochemically active Li_yNiO_x. The probable cause of Li_yNiO_x formation is explained by the disordered structure and containing empty spaces for Li^+ ions of electrochromic NiO.

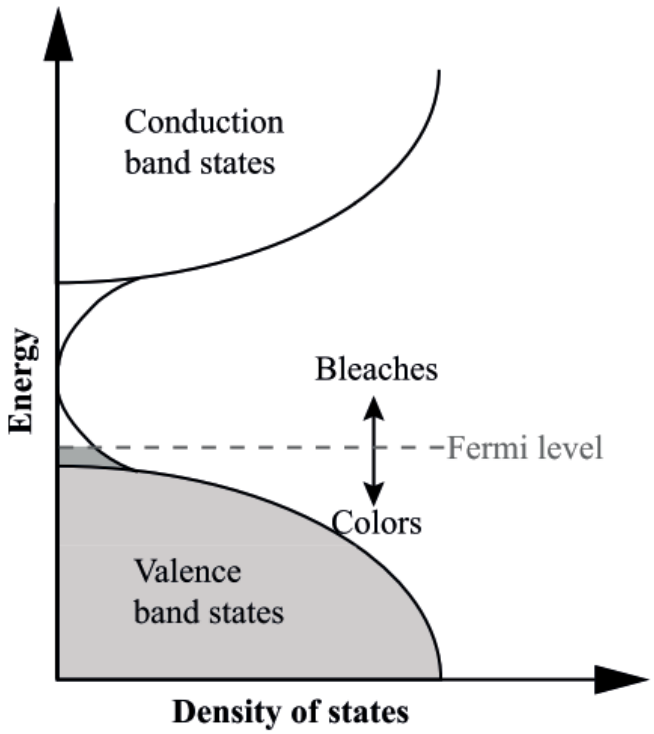

Figure 2.3: An illustration of the band structure of nickel oxide and the variation of the Fermi level as charge is intercalated (bleached) and deintercalated (colored) [93].

However, regardless of which ion is used, intercalation of charges leads to the emergence of new localized energy states near the valence band and. The Fermi level moves towards lower energies and higher energies by electron extraction and insertion, respectively. This Fermi level movement leads to the transformation of the material between bleached and colored with absorption that is due to transitions between localized sites. These transitions these being intervalence charge transfers between Ni^{2+} and Ni^{3+}. An illustration of relation between band structure of NiO and change in Fermi level by charge intercalation/deintercalation is given in figure 2.3. If Fermi level shifts to the valance band state, optical absorption increases and coloration of NiO films occur.

3. THIN FILM DEPOSITION TECHNIQUES

Thin film deposition is the technology of coating a very thin film of material between a few nanometers to 100 micrometers, or onto a coating to form multilayers. Thin-film deposition is used in the manufacture of semiconductors, solar panels, disk drives, and optical devices. There are two major categories for making thin films as physical and chemical deposition. These two major thin film deposition techniques were categorized in Table 3.1.

Table 3.1: Thin film deposition techniques.

Category	Method	Variety
Chemical	Gas-phase	Chemical vapor deposition Atomic layer deposition
	Liquid-phase	Sol-Gel Chemical bath deposition Electrodeposition
Physical	Evaporation	Electron beam Thermal
	Sputtering	RF/DC Magnetron Reactive

3.1 Chemical Thin Film Deposition Techniques

Methods of forming films by chemical processes in the gas phase include chemical vapor deposition (CVD) and atomic layer deposition (ALD).

3.1.1 Gas phase

Chemical Vapour Deposition (CVD): CVD is a method of coating a material vapor by chemical reaction occurring on a heated substrate surface. Both simple and complex compounds in thin film form can be synthesized at low temperatures with CVD. The composition and physical properties can be tailored by control of experimental

conditions such as substrate material, substrate temperature, the composition of reaction gas mixture, total pressure, etc.

Atomic Layer Deposition (ALD): ALD is based on the sequential release of chemical reactants gas pulses to deposit a thin film in a layer-by-layer fashion. ALD has an importance in semiconductor and energy technologies. The ALD method gains importance due to its suitability and control over material thickness and composition when smaller, i.e. atomic sizes and preferential arrangement are required in the devices to be produced.

3.1.2 Liquid phase

Sol-Gel: The term sol-gel is an amalgamation of two terms solution and gelation. This process involves the formation of a liquid suspension (sol), a stable colloid solution obtained by hydrolysis and condensation of precursors to form metal-oxygen-metal bonds (M-O-M). The condensed sol particles form a 3D network called gel. By processing the sol, it is made possible to produce thin films of materials. It is possible to create thin films with controllable chemical composition to be produced with this technique.

Chemical bath deposition: The substrate is dipped into the solution of the material whose thin film is desired to be formed. The properties of the thin films formed vary with the pH value of the solution, ambient temperature, reaction types and times, and viscosity.

Electrodeposition: This tecnique is the process of thin-film deposition on a substrate with electrochemically reduction of metal ions contained in an electrolyte. It is possible to deposit both organic and inorganic thin films with electrodeposition. In this tecnique, the cathode (working electrode), anode (counter electrode) and the electrolyte solution in which the base is immersed with these electrodes are used. By using flow of electrical current, metal ions are to be reduced. At the end of this process, a thin film is deposited on the surface. This technique is low cost and well suited for wide area applications.

3.2 Physical Deposition Techniques

3.2.1 Evaporation

Electron beam (e-beam) evaporation: Electron Beam Evaporation is a type of physical vapor deposition by bombarding the material to be coated with electrons extracted from the tungsten filament to be evaporated and deposited on the substrate. This process takes place in a vacuum environment. This method can be used to create multilayer thin films of different materials, so it is suitable for coatings to be formed by various masking methods. Electron beam evaporation can be applied to all metals and alloys, especially for materials that have high melting points. And also because of its high degree of control of deposition rate that may affect thin film structural properties, it can be used in so many different fields of thin-film deposition.

Thermal evaporation: In thermal evaporation, the target material evaporates in a vacuum environment due to high-temperature heating, and the vapor particles become solid on the substrate, forming a thin film. With this technique, it is possible to create thin films of a wide variety of materials such as metal, semiconductor, or composite materials. Generally, the energy of ions impinging the surface of the substrate is very low, and therefore it is necessary to heat the coated substrate to high temperatures. The microstructure of the thin films formed at the end of the coating process is substantially different from the evaporating bulk material.

3.2.2 Sputtering

Since thin films are prepared using sputtering method, within the scope of the thesis, detailed information about this method is given in this section. In the sputtering process, when the target surface formed from the material to be coated is bombarded with energetic ions, the surface atoms of the target are ejected from the surface due to transfer of momentum and kinetic energy from collisions between surface atoms and energetic particles.

The illustration of sputtering deposition is given in figure 3.1. The principle of this process is to use the energy of plasma phase (ionized gases) of a target material and to deposit the surface atoms of target on a substrate in a vacuum environment. To make sputtering process in a vacuum environment provides to enhance using minimum

energy, increasing mean free path between collision particles and preventing unnecessary crashings.

Sputtering is a process performed at low pressures because the mean free path of the particles is larger compared to the dimensions of the vacuum chamber. This pressure is provided by mechanical and turbo molecular pumps connected to the vacuum system. Argon which is inert gas is generally used as sputtering gas because they do not react with other materials.

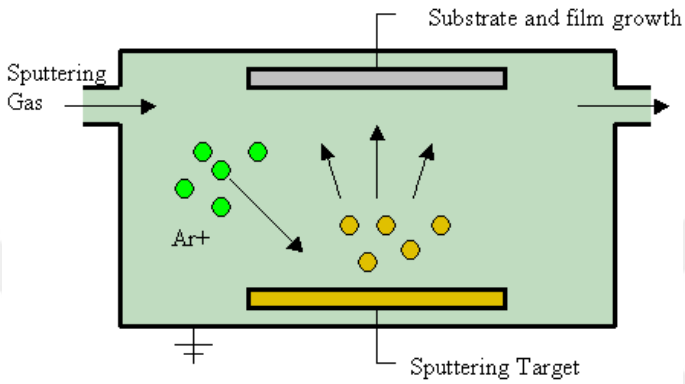

Figure 3.1: The illustration of sputtering process.

The sputtering process provides a controlled thin film coating by changing parameters such as gas pressure, the distance between the sputtering system and the target, and sputtering power. With this technique, coating of very large areas and industrial coatings can be produced, the substrate material can be cleaned by ion bombardment before coating and the adhesion, strength, and structural properties of the coating can be changed, materials with high melting temperatures or dielectric materials can be deposited [94]. The sputtering technique is basically classified as direct current sputtering (DC), radio frequency (RF) sputtering, and magnetron sputtering method. These sputtering processes depend on the type of material to be used as the target material and the power source used.

3.2.2.1 DC sputtering

The important advantages of realizing the sputtering process with the DC power supply are that it enables low cost and controlled thin-film coatings. In the DC Sputtering coating system, the target material (cathode) to be coated is placed parallel to the substrate (anode). A DC electrical current (in -2 to -5kV range) is applied to the

cathode and a positive charge is applied to the substrate. Because of collisions between the inert gas atoms and free electrons in the plasma, the gas atoms will be ionized. Positively charged ionized particles will move directly towards the target material due to the electronic field generated by DC, causing the atoms within it to eject. The ejected atoms condensed at the substrate surface, forming thin film of target material. DC sputtering is a suitable method for coating many metallic materials. However, during coating of dielectric materials, it is one of its limiting features that it causes arcing and poisoning, which causes the coating process to stop. or this reason, it is not preferred for coatings of insulating materials.

3.2.2.2 RF sputtering

Since it is not possible to apply the acceleration potential directly to the insulator surface, the insulators cannot be sputtered with the DC sputtering technique. In this case, the positive charge to be accumulated during ion bombardment cannot be neutralized. In the RF sputtering technique, this situation is solved by applying a high frequency potential to the metal conductive electrode behind the insulating target. The target is metallized by placing a chrome-copper film behind the target to be sputtered. By altering the polarization of the cathode material by alternating current (AC), the target is bombarded with ions and electrons sequentially and continuously. Therefore, the positive charge will be neutralized by the electrons and sputtering may occur as the insulating target will be bombarded with ions and electrons. RF sputter technique is most widely used because it can be used for both conductive and non-conductive targets. AC sputtering is usually performed at the 13.56 MHz frequency level [95].

3.2.2.3 Magnetron sputtering

Magnetron sputtering technique is the most preferred deposition type industrially for making coatings with homogeneous and well-adhered deposition over a large area. It offers great advantages such as ease of selection of target material with very high melting points, high deposition rate, and also ease of thickness control [96]. The restriction of low ionization efficiencies in plasma in basic sputtering deposition was solve with the discovery of magnetron sputtering. A magnetic field created parallel to the target surface limits secondary electron movement, which increases the probability of ionizing electron-atom collisions in nearby of target. In this thesis, RF magnetron reactive sputtering technique was used to create NiO films on ITO/glass substrate.

3.2.2.4 Reactive sputtering

It is a method of sputtering by adding a reactive gas species such as oxygen or nitrogen along with inert argon to the vacuum chamber to obtain oxide or nitride films from the target material [97]. During deposition, reaction happens on target and substrate surfaces. The structural, optical, and electrical properties of metal-oxide thin films which are deposited with reactive sputtering method influenced by ratio of reactive gas. The reactive gas ratio effect on properties of thin films is one of the research fields of focused on in literature. The reactive gases used and the most common compounds sputtered in reactive gas sputtering technique are briefly listed [98]:

- Nitrides (nitrogen, ammonia) - TiN, AlN, Si_3N_4,
- Oxides (oxygen) - Al_2O_3, In_2O_3, SnO_2, SiO_2, Ta_2O_5
- Carbides (methane, acetylene, propane) - TiC, WC, SiC
- Oxycarbides and oxynitrides of Ti, Ta, Al, and Si

A change in reactive gas content causes a change in sputtering rate. This phenomenon can be explained with a typical hysteresis curve for thin films deposited from $NiV_{0.8}$ target in a study of Avendano et al. (as given in figure 3.2) [99].

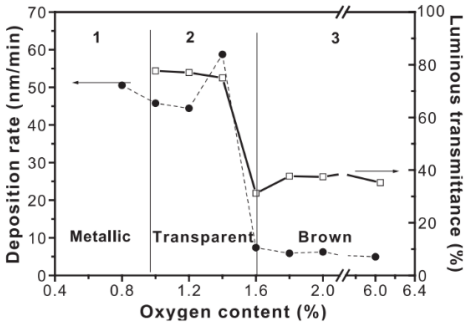

Figure 3.2: Deposition rate and transmittance vs. oxygen content.

There are three distinct deposition regions in the hysteresis curve in the Ar plasma with different amounts of oxygen. In region 1, the thin films evolve nearly metallic with increasing oxygen content in Ar plasma. With further increasing of oxygen ratio, deposition rates abruptly decrease and the films were evolved to be transparent and suboxide in region 2. Then above a critical oxygen content (limit value between region 2 and region 3), the films were oxidized with low deposition rates and low transmittances.

4. ELECTROCHEMICAL CHARACTERIZATIONS

The most basic method used to investigate the electrochromic properties of thin films is electrochemical characterization techniques. Therefore, electrochemical methods used in this thesis will be discussed in this section. Electrochemistry is a method of studying reactions involving electron transfers that relate the flow of electrons to chemical changes such as the oxidation or reduction of a metal complex. In order to observe the electrochromic effect, redox reactions must occur with the diffusion of ions and electrons into the thin film.

The three-electrode cell used to do this process is illustrated in figure 4.1. A potential applied between the reference electrode (RE) and working electrodes (WE) causes a current between the counter electrode (CE) and working electrode (WE). Generally, electrode materials are as follows: standart hydrogen electrode (SHE), saturated calomel electrode (SCE) or silver/silver chloride (Ag/AgCl) as reference electrode and platinum (Pt), gold (Au) or graphite as counter electrode. This three-electrode measurement cell provides to determine electrochemical properties of electrochromic thin films and because of this reason, it is called as 'Electrochromic Half-Cell' in literature.

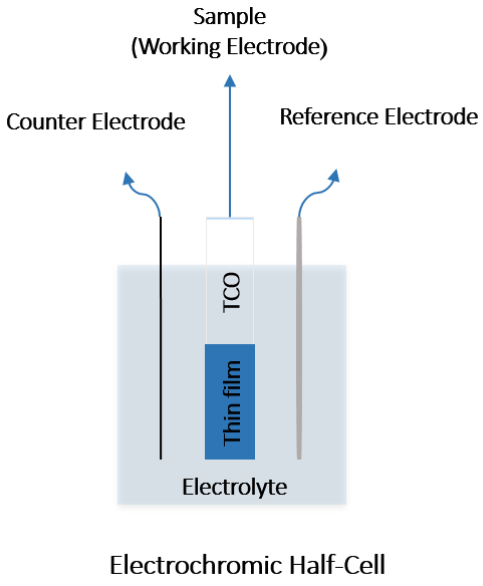

Figure 4.1: Illustration of three-electrode cell.

4.1 Cyclic Voltammetry

Cyclic voltammetry (CV) is a powerful electrochemical technique widely used to study reduction and oxidation of molecular species and electron transfer initiated chemical reactions involving catalysis. In this method, like other voltammetric methods, a three-electrode setup including a working electrode, a reference electrode, and a counter electrode is used. For cyclic voltammetry measurement, the three-electrode system is placed in the electrolyte solution that is ion storage. Then, the potential between the working and reference electrodes is changed linearly until it reaches a certain potential, after which it scans back in reverse direction to return to the first applied potential by using a potentiostat. The potential is changed with time which is called scan rate. These potential cycles could be repeated for many times as needed. The current observed at the working electrode is plotted versus the applied voltage (i.e. working electrode potential), creating a cyclic voltammetry graph. The illustration of a typical cyclic voltammetry graph is given in figure 4.2. The oxidation and reduction potentials can be found by CV analysis. These cathodic or anodic peak potentials belong to the redox reactions vary depends on the type of material.

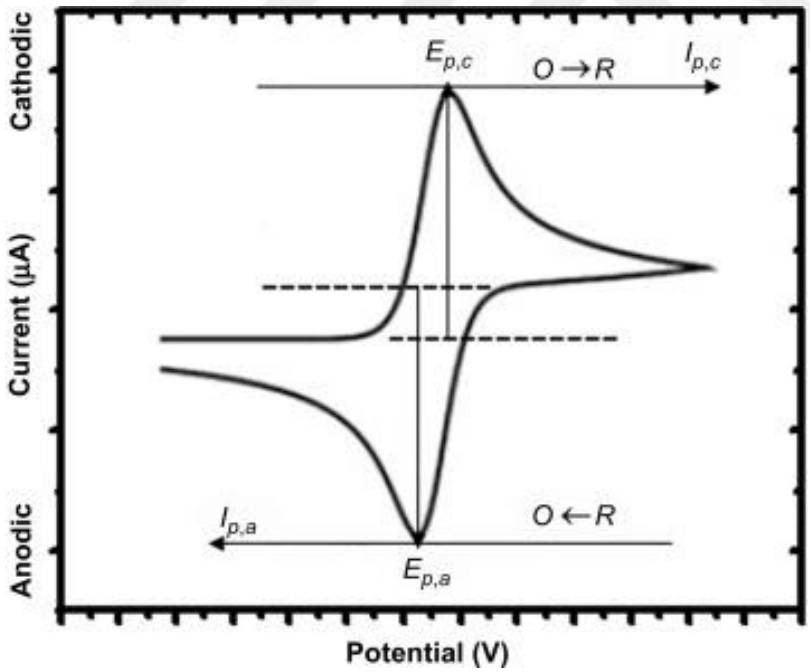

Figure 4.2: The illustration of a typical cyclic voltammetry graph [100].

With the CV method used to make electrochromic tests of a material, it is possible to find the redox potential, the amount of charge entering the thin film matrix, and the diffusion coefficient.

4.2 Chronoamperometry

Chronoamperometry (CA) is a method that enables the measurement of the diffusion process with time dependent square wave voltage applied to the WE. In this technique, the applied step potential is constant as it can be positive or negative. The redox reactions take place, and current flows through the working electrode is obtained depending on time. This process enables to easily find the coloration/bleaching times and the amount of charge into/out to the thin film matrix.

The illustration chronoamperometry response is given in figure 4.3. The red areas give the amount of charges as mentioned before. From the time (t) variation in current density (J) curves in figure 4.3, the amount of charge inserted (Q_{in}) and extracted (Q_{out}) into/out the NiO films can be deduced by the integration of the curves within the coloration or bleaching time with subjected to equation 4.1:

$$Q = \int_{t_1}^{t_2} J(t)dt \tag{4.1}$$

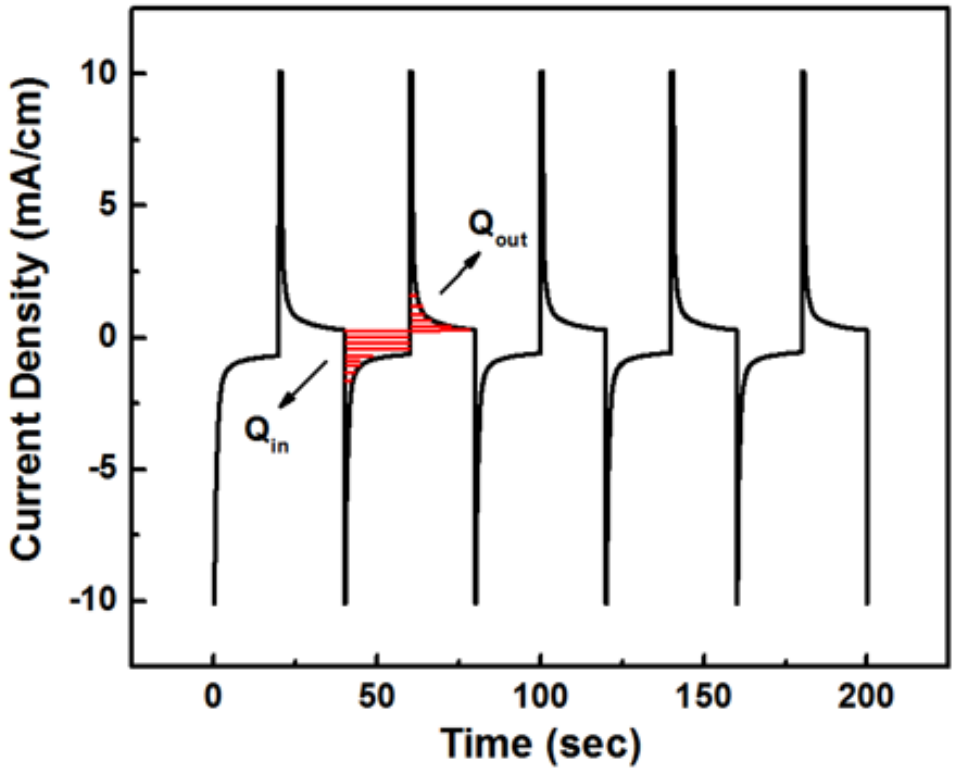

Figure 4.3: The illustration of chronoamperometry graph.

5. EXPERIMENTAL PROCEDURE

5.1 Film Deposition

In this thesis, the nickel oxide thin films were deposited with reactive RF magnetron sputtering system. A pure nickel metal target with 2" diameter was used and the distance between substrate and target was kept constant as 7.5 cm. The NiO thin films were coated on ITO-coated glass substrates at room temperature. The thickness and sheet resistance of ITO were 250±5 nm and 16-17 Ω/sq, respectively. In order to examine how RF magnetron sputtering parameters affect the electrochromic behavior of NiO thin films, three sets of experiments were made for different oxygen contents, growth powers, and growth pressures. The deposition conditions of these sets of experiments are as given in Table 5.1. The thicknesses were tried to be kept constant for each set as 150±30 nm to avoid thickness effect.

Table 5.1: Deposition conditions of NiO thin film with different growth powers, pressures, and oxygen contents.

Parameters	Condition 1	Condition 2	Condition 3
O_2 / Ar + O_2 (%)	50, 60, 70, 90	90	90
Growth Power (W)	60	60, 75, 90, 105	90
Growth pressure (mTorr)	13	13	10, 13, 17, 25

5.2 Optical Measurements

The transmittances of as-deposited NiO thin films were measured by Lambda 1050 model Perkin Elmar UV/VIS/NIR spectrophotometry at wavelength range of 280-2500 nm. Hitachi U-2900 model UV-Solution spectrophotometry was used to determine the transmittances of thin-films depends on time (at constant wavelength of 630 nm). The Sentech 900 ellipsometry system was used to obtain the refractive index (n) and extinction coefficient (k), which are optical constants. By using refractive index at a constant wavelength of visible spectral range, the surface porosities of NiO films deposited at different sputtering conditions were calculated with the equation 5.1

where refractive indices of n_f : film, n_b : bulk, and n_{air}: air [101]. The refractive index at a wavelength of 630 nm is 2.18 for bulk NiO.

$$Porosity\ (\%) = 100\ x\ \frac{(n_f - n_b)}{(n_{air} - n_b)} \tag{5.1}$$

5.3 Electrochemical Measurements

The three-electrode cell was used to determine electrochemical properties of NiO films. In the three-electrode cell, platinum (Pt) wire as counter electrode, Ag/AgCl as reference electrode, and NiO films coated on ITO/glass substrates were used as working electrode in the electrolyte.

For the preparation of electrolyte used in the cell, $LiClO_4$ powder was dissolved in propylene carbonate (PC) at room temperature and the electrolyte molarity was set as 1 M.

Electrochromic measurements have been done with the CHI 6005D model CH Instrument electrochemical measurement device. For the measurement of cyclic voltammetry, a linear potential sweep between -1.5 V and 1.5 V at 0.1 V/s scan rates was used for all NiO films. CV was performed for 20 cycles for preliminary experiments due to the activation procedure of NiO thin films.

Chronoamperometry measurements were performed with applied voltage of +1.5 V and -1.5 V (vs Ag/AgCl), the pulse width is 20 s, for 5 cycles. The three-electrode cell has been placed at spectrophotometry and the in-situ transmittances were measured with CA, simultaneously.

5.4 Structural and Morphological Measurements

Panalytical Empyrean model X-ray Diffraction device with Cu K_α (λ = 1.5405 Å) was used for characterization of the crystallographic structure of NiO films. X-ray reflectometry (XRR) was used to find the density of films.

The surface morphologies of NiO films were analyzed by Veeco Dimension 3100 model Atomic Force Microscopy (AFM) device and Hitachi SU8220 model Field Emission Gun Scanning Electron Microscopy (FEGSEM) device.

6. RESULTS AND DISCUSSION

The results of the experiments were given in this section.

6.1 Effect of the Oxygen Partial Pressure on the Electrochromic Properties of NiO

In this section, nickel oxide thin films were deposited by reactive RF sputtering at room temperature with the different ratio of oxygen partial pressures (O_2/O_2+Ar % oxygen content in sputtering atmosphere) and their electrochromic properties were examined.

In order to examine fully oxidized NiO thin films from a metallic target of Ni, in addition to inert gas argon, oxygen was used as a reactive gas under constant pressure 13mTorr (1.73 Pa) and growth power 60W. The variation of the deposition rate with oxygen content (O_2/O_2+Ar %) in the sputtering atmosphere was measured. According to the measurement, three different deposition regions were distinguished as shown in figure 6.1, as explained in section 3.2.2.4. The oxide region shows the most efficient oxygen content values to examine NiO thin films.

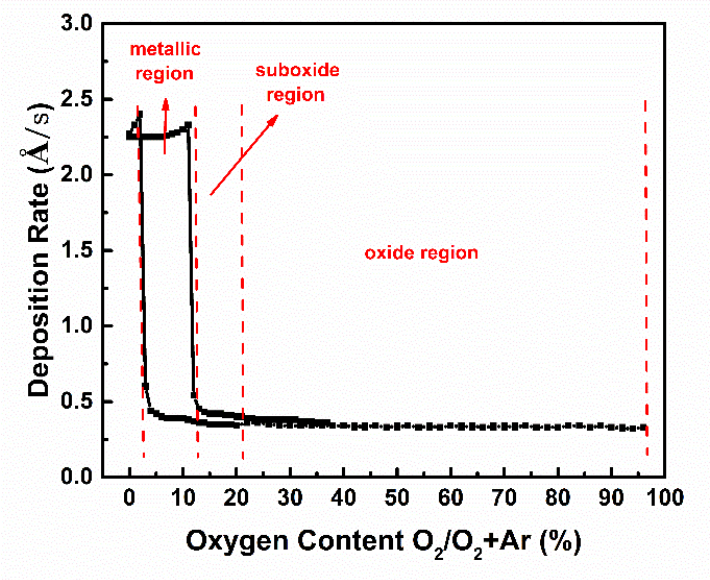

Figure 6.1: Deposition rate for as-deposited NiO films versus oxygen content in the sputter plasma. Vertical lines signify different visual appearances.

According to the results of this hysteresis experiment, the required oxygen content to examine fully oxidized NiO films were observed to be varied from 40% to 90%. However, 40% oxygen content is in critical level to obtain full oxide films, films were deposited under oxygen contents varied from 50% to 90%.

ITO films with 0.8x1.25 cm^2 area and 16-17 Ω/sq sheet resistance were used as substrate. The growth power and pressure were individually kept at 13mTorr and 60W. The working pressure was measured by sensors in vacuum chamber.

Film thicknesses measured with the Dektak Vecoo profilometer and were found 150 nm (±10nm). The coating parameters were presented in Table 6.1.

Table 6.1: Coating parameters of NiO films grown at different oxygen contents in sputtering atmosphere.

Ar:O_2 Ratio (%)	Growth Power (Watt)	Pressure (mTorr)	Working Pressure (mTorr)	Ar:O_2 Ratio (sccm)	Thickness (nm)
50 : 50	60	13	8.25	2.4 : 2.4	153
40 : 60	60	13	8.52	2.0 : 2.9	155
30 : 70	60	13	8.45	1.4 : 3.3	141
10 : 90	60	13	9.50	1.1 : 4.7	145

The purpose of this study to clarify the effects of oxygen partial pressure on optical and electrochromic properties of NiO films and determine the most efficient oxygen content in sputtering atmosphere for the next experiments.

The optical transmittance spectrum of as-deposited NiO films deposited on ITO/Glass substrate with various oxygen contents was given in figure 6.2. There is a low increment in transmittance variation observed depending on oxygen content.

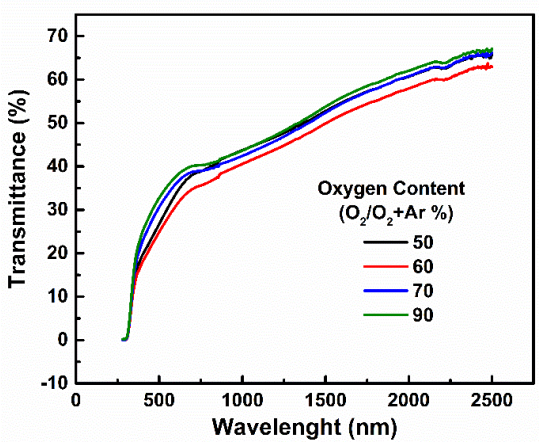

Figure 6.2: The optical transmittance spectrum of as-deposited NiO films deposited on ITO/glass substrate with various oxygen contents.

The crystalline structures of NiO films were confirmed by XRD. Figure 6.3 shows the XRD patterns of ITO/glass substrate and NiO films deposited on ITO/glass substrates with various oxygen contents (O_2/O_2+Ar %). Besides peaks associated with ITO structure, there are three diffraction peaks observed at $2\theta \approx 36.9°$, 42.7° and 62.1°, along (111), (200), and (220) planes, corresponding to a cubic NiO phase (JCPDS 22-1189). So a polycrystalline nature was obtained for samples prepared with oxygen content.

Figure 6.3 shows that the difraction peaks slightly shifted toward a higher angle with increasing oxygen content.

It was observed that the 2θ position of the preffered (111) oriantation shifted from 36.52° to 36.92° and (200) oriantation shifted from 42.5° to 42.72° as the oxygen content gradually increased. It could be ascribed to the presence of the lattice strain in the sputtered films.

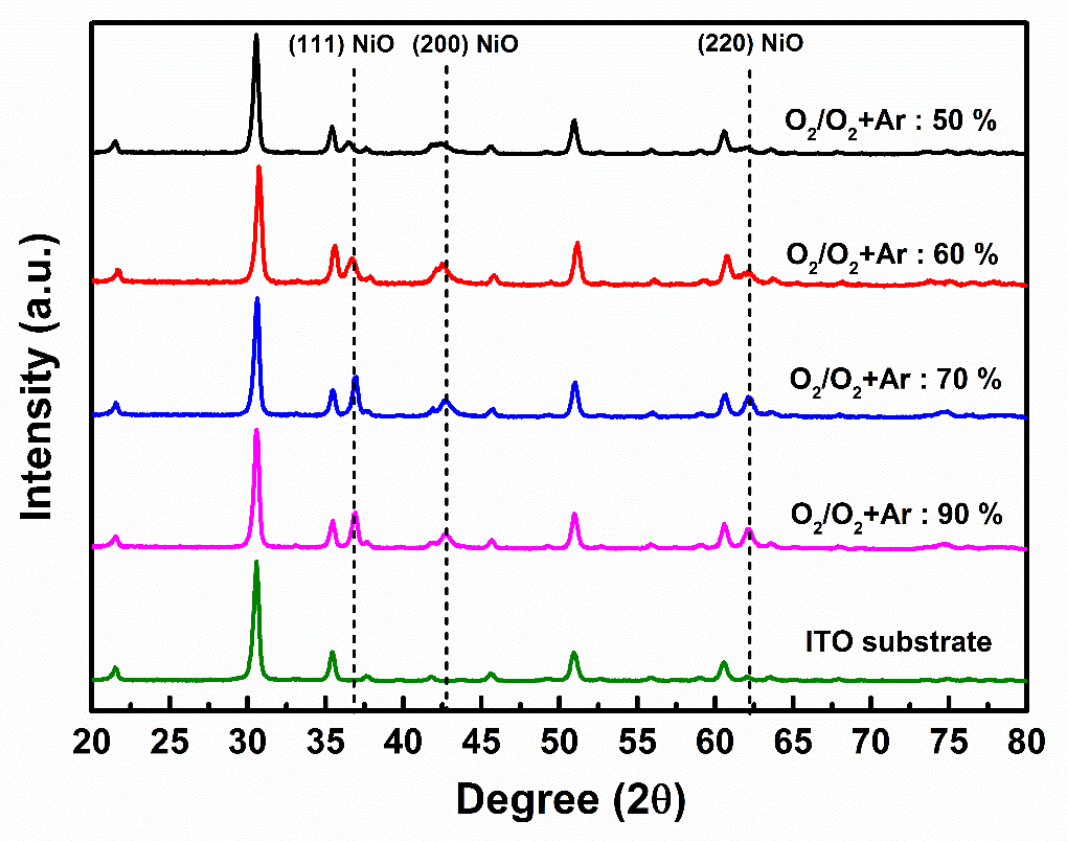

Figure 6.3: XRD patterns of ITO/glass substrate and as-deposited NiO films deposited with various oxygen contents (O_2/O_2+Ar %) on ITO/glass substrates.

The surface morphologies of NiO films were analyzed by AFM and SEM. Figure 6.4 shows the 2D AFM images of NiO films deposited at different oxygen contents, in the scan range of 1 μm x 1 μm.

The images reveal a smooth surface morpology and deposited NiO particles are distributed uniformly over the entire scan region. It can be say that the grain sizes were decreased with increasing oxygen content from the figure 6.4. The increased oxygen content causes formation of more defects, oxygen interstitials, nickel vacancies and causes variation in grain size values [18][103].

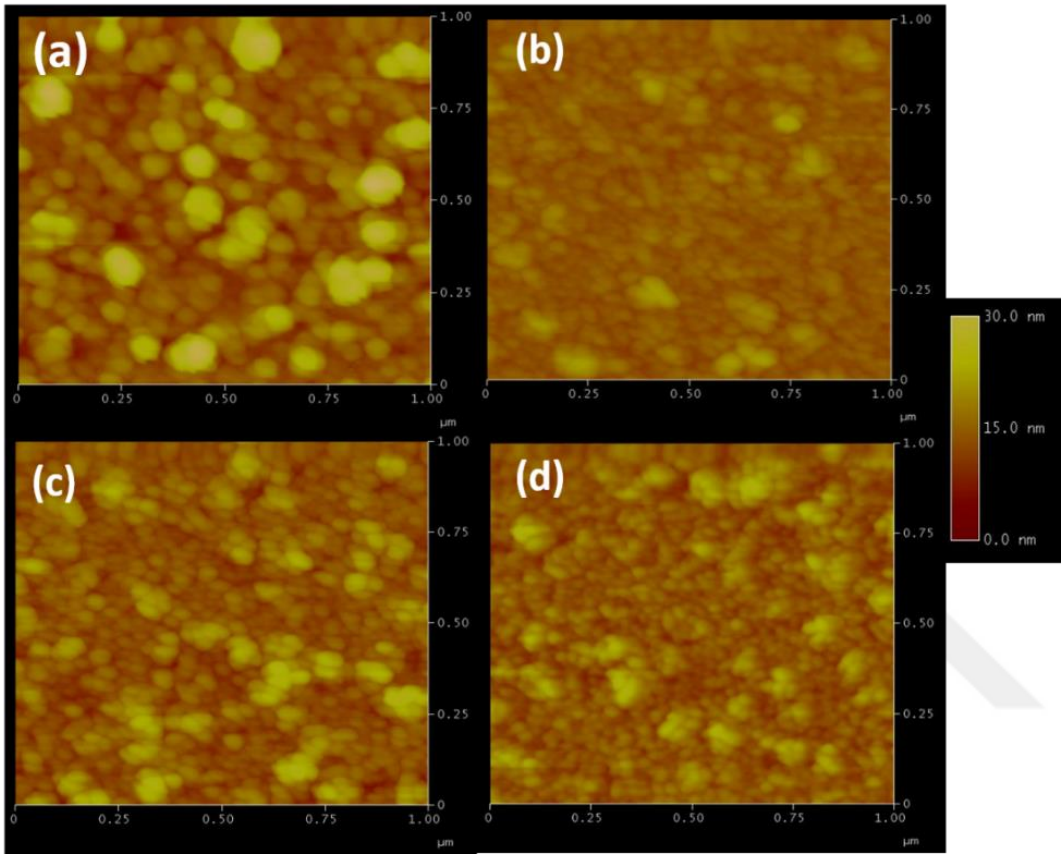

Figure 6.4: The two dimensional 1x1 µm AFM micrographs for the NiO films deposited with various oxygen contents (O_2/O_2+Ar %) on ITO/Glass substrates (a) 50% O_2 (b) 60% O_2 (c) 70% O_2 (d) 90% O_2.

The roughness values of NiO films deposited with various oxygen contents were given in Table 6.2. Results have some differences but they are not a significant roughness change.

Table 6.2: Roughness values of NiO films deposited with various oxygen contents (O_2/O_2+Ar) deposited on ITO/Glass substrates..

Oxygen Content (%)	R_q (nm)
50	3.77
60	3.49
70	3.89
90	3.45

The plan view and cross-section SEM images of the films were presented in figure 6.5. The scale bar of SEM images is 1µm, the scale bar of inset figures is 200nm. With

increasing oxygen content from 50% to 60%, the surface morphology of the films has become triangular features with linear extension. It was observed that the grain sizes were decreased with increasing oxygen content. Cross-section SEM image of the film deposited with 50% oxygen content shows that the film is approximately 144 nm thick (shown in figure 6.5 (e)) which is very close to the measurement result of the profilometer.

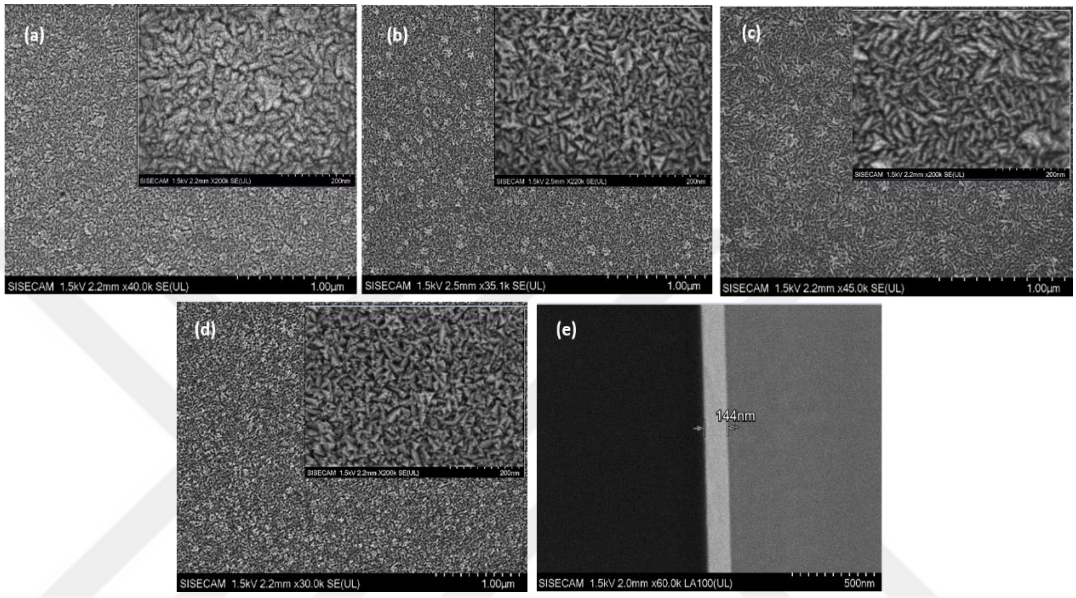

Figure 6.5: SEM images for NiO films deposited with various oxygen contents (O_2/O_2+Ar %) on ITO/Glass substrates (a) 50% O_2 (b) 60% O_2 (c)70 % O_2 (d) 90% O_2 (e) cross-section SEM image for NiO film deposited with 50% O_2 on glass substrate.

For the CV of NiO film, cathodic peaks are attributed to the reduction of Ni^{+3} to Ni^{+2} by the insertion of Li^+ ions into the crystal structure of nickel oxide that is attributed to the formation of different crystalline phases of $LiNiO_x$. On the other hand, anodic peaks are corresponded to oxidation of Ni^{+2} to Ni^{+3} by the extraction of Li^+ ions from the crystal structure of the NiO during charging. These transformations imply the coloring and bleaching of NiO_x films in the electrolyte as subjected to the following equation 6.1 and equation 6.2 [104]:

$$NiO_x + yLi^+ + ye^+ \rightarrow Li_yNiO_x \quad (activation\ procedure) \tag{6.1}$$

$$\underset{colored\ (brownish)}{Li_yNiO_x} \leftrightarrow \underset{bleached}{Li_{y-z}NiO_x} + zLi^+ + ze^- \tag{6.2}$$

Reaction in equation 6.1 describes the 'activation' procedure of NiO films and reaction in equation 6.2 describes the reversible intercalation/deintercalation process which is associated with the electrochromic effect on NiO [105]. Because of the necessity of

the activation procedure, all experiments were performed after 30 cycle CV experiments. The activation procedure of NiO was argued by Liu et al. [106] and explained in section 2.3.

CV was performed with linear potential sweep between -1.5 V and 1.5 V at 0.1 V/s scan rates in 1M $LiClO_4$-PC electrolyte for all films (given in figure 6.6).

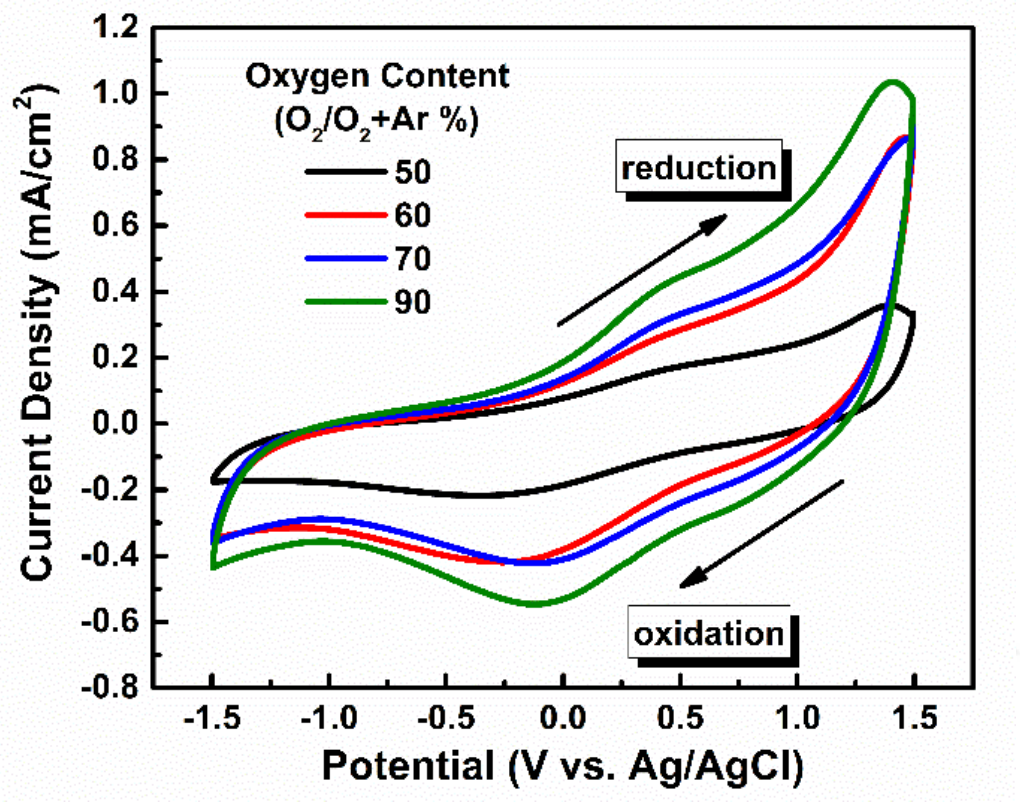

Figure 6.6: Cyclic voltammetry curves of NiO films deposited with various oxygen contents (O_2/O_2+Ar %) on ITO/glass substrates.

As deposited films were dark brown. During the anodic scan from 1.5 V to -1.5 V, the current was started the flow caused the bleaching of the films and curve-shaped peaks were observed. With the applying reverse potential from -1.5 V to 1.5 V, the cathodic current was started to flow caused the coloring of the films. A change in the current density of oxidation and reduction processes causes the change in the amount of charge inserted/extracted into/out the film. Higher current density values indicate that the films have a higher charge capacity [4][5].

With the change in oxygen content in the sputtering atmosphere from 50% to 90%, there is a significant rise in the current density values for both anodic and cathodic scan. The maximum cathodic and anodic currents were observed as 1.035 mA and -0.5467 mA at 1.405 V and -0.0115 V for the film that was deposited with 90% O_2

respectively. The results show that the film deposited with 90% O_2 has the highest charge capacity.

CA measurements were performed for applied voltage of +1.5 V and -1.5 V (vs Ag/AgCl), pulse width is 20 s, for 5 cycles in 1M $LiClO_4$-PC electrolyte. The in-situ transmittance of NiO films at a wavelength of 630nm was measured with CA, simultaneously. Figure 6.7 shows the (a) CA curves, (b) in-situ transmittance results, and (c) optical modulation values (at a constant wavelength of 630nm) of NiO films deposited with various oxygen contents. From the time (t) variation in current density (J/cm^2) curves in figure 6.7 (a), the amount of charge inserted (Q_{in}) and extracted (Q_{out}) into/out NiO films was deduced with subjected to the equation 4.1. The response times of the films were determined from the transmittance-time graph in figure 6.7 (b).

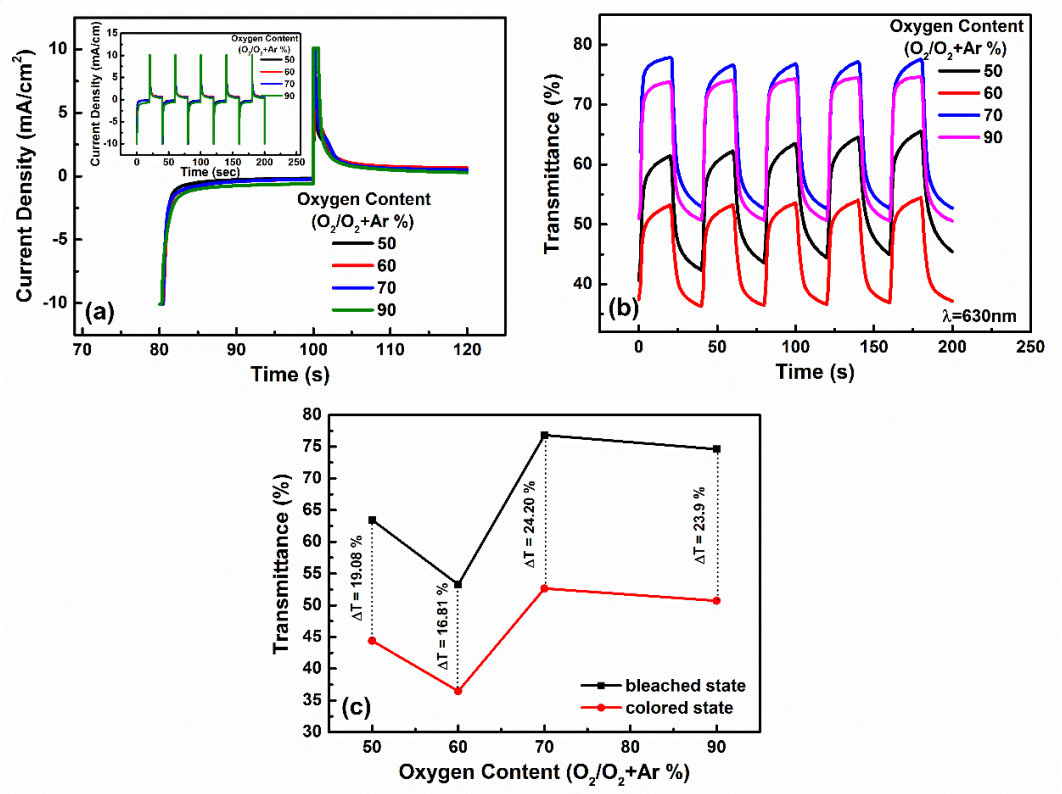

Figure 6.7: (a) Time response of the current density (Inset shows the plot of CA for 5 cycles) (b) in situ transmittance at 630 nm in five CA cycles (c) the bleached and colored state trasmitances and optical modulations of NiO films deposited with different oxygen contents.

The calculated amount of charges inserted/extracted (Q_{in}/Q_{out}) into/out to films, the response times according to chronoamperometry, and transmittance-time measurements were given in Table 6.3.

Table 6.3: The amount of charges inserted/extracted to the films, reversibility, and response times of NiO films deposited with various oxygen contents (O_2/O_2+Ar %).

Oxygen Content (%)	Q_{in} mC	Q_{out} mC	Bleaching Time (s)	Coloration Time (s)
50	5.811	5.704	10	15
60	11.399	10.721	10	12
70	10.967	10.272	9	12
90	13.502	12.147	6	10

The amount of charges (Q_{in}, Q_{out}) were increased with increasing oxygen content from 50% to 90% as given in Table 7.3. Since the film coated with 90% oxygen allows the easiest ion diffusion. These results show that NiO film deposited with 90% O_2 has the biggest charge capacity.

Figure 6.7 (c) shows the colored/bleached state transmittances and optical modulations (ΔT). From the transmittance-time measurements, optical modulation values were varied between 16.81% to 24.20%. The highest optical modulation was observed for the film deposited with 70% O_2 as 24.2%, but this value is so close to the optical modulation of the film deposited with 90 O_2 as 23.9%. Therefore, other parameters were also investigated to compare electrochromic performances of NiO film deposited with various oxygen contents.

Another important parameter to determine which film has the best electrochromic behavior is the response time of the films. Response time is the time required for the bleaching/coloring process to occur. The response times were determined from the time-dependent transmittance graph in figure 6.7 (b) and given in Table 6.3. The bleaching time was decreased from 10s to 6s and coloration time was decreased from 15s to 10s with increasing O_2 from 50% to %90. It is indicating that the excess interstitial oxygens make easy the ion intercalation/deintercalation during the coloring/bleaching processes. It was observed that films deposited with higher oxygen contents had faster responses which confirms the easier insertion of the Li^+ ions to the NiO film. Therefore, the fastest bleaching/coloring process occurred for film deposited with 90% O_2. Another remarkable result is that the response time during the coloring process is in any case higher than the response time during the bleaching process. It may be explaine with the amount of extracted charge is not as same as the amount of

inserted charge (as given in Table 6 .3). Ion trapping may prevent the outward diffusion required for coloration and slows down the process.

It has been widely observed in other electrochromic studies, the film density and the surface porosity are the critical values for electrochromic performances of the thin films [107]. If the film density is low and surface porosity is high, ion diffusion can be facilitated. The refractive indices (n) of as deposited NiO films on glass were obtained from ellipsometry measurements. By using the refractive indices, corresponding surface porosity values were calculated using equation 5.1. An also, the density of the films was determined from XRR results. The change in the film density, refractive index (n), and surface porosity depending on the oxygen content was presented in figure 6.8. The refractive index of films was decreased from 1.99 to 1.85 and corresponding surface porosities were increased from 15.49% to 27.68% with increasing O_2 from 50% to 90%. And also, the film densities decreased with increasing O_2. The density and the porosity were correlated with each other as expected.

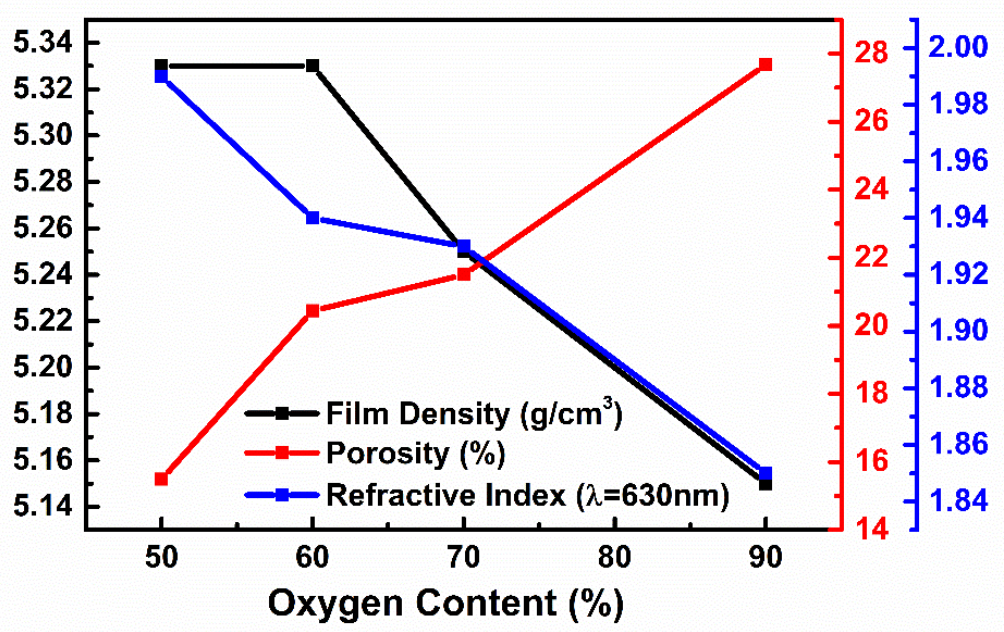

Figure 6.8: Film density, refractive index (at 630nm) and surface porosity of as-deposited NiO films on glass with various oxygen contents.

As overviewed above, the improvement in electrochromic properties of NiO films with increasing oxygen content can be explained by an increment of porosity of the films. Increment of oxygen content in sputtering atmosphere caused the increase in porosity of the films and a decrease in film density. Therefore, higher porosities caused an increase in the amount of ions inserted into film matrix. The ease of ion insertion in

high porosity films causes a decrease in response times and also an improvement in charge capacity and optical modulation of the nickel oxide films. Based on these results, 90% oxygen content was chosen for the next experiments.

6.2 Effect of Growth Power on Electrochromic Properties of NiO

In this section, thin films of Ni oxide were deposited by reactive radio frequency RF sputtering at 60, 75, 90, and 105 W, and their electrochromic properties were examined. The purpose of this study to clarify the effects of RF growth power on the optical and electrochromic properties of NiO films and determine the most efficient growth power for the next experiments. NiO films were deposited on ITO films with 0.8x1.25 cm^2 and 16-17 Ω/sq sheet resistance at different growth powers varied from 60 to 105W.

The pressure and oxygen content were individually kept at 13 mTorr and 90 %. The working pressure was measured by sensors in the vacuum chamber.

Film thicknesses were measured with the Dektak Vecoo profilometer and all were found 150 nm (±15nm). The coating parameters were presented in Table 6.4.

Table 6.4: Coating parameters of NiO films deposited at different growth powers.

Growth Power (Watt)	Pressure (mTorr)	Working Pressure (mTorr)	Ar:O_2 Ratio (%)	Ar:O_2 Ratio (sccm)	Thickness (nm)
60	13	1.13	10 : 90	1.1 : 4.7	137
75	13	1.15	10 : 90	1.1 : 4.7	152
90	13	1.12	10 : 90	1.1 : 4.7	155
105	13	1.10	10 : 90	1.1 : 4.7	144

The growth power induced change in optical transmittance of NiO films deposited on ITO/Glass substrate with various growth powers is shown in figure 6.9. Initially, the film deposited at 60W have shown a transmittance of 38% at 630 nm in the visible region.

At higher sputter powers, kinetic energy of sputtered gas molecules is high aand inert argon gas molecules dominate during the growth process. In this case, deposited NiO film contains less number of oxygen interstital defects.,

Therefore, the change in transmittance were probably attributed to the microstructural change in NiO film and the decrease of interstitial atoms in films which would cause to scatter or absorb the incident light [108].

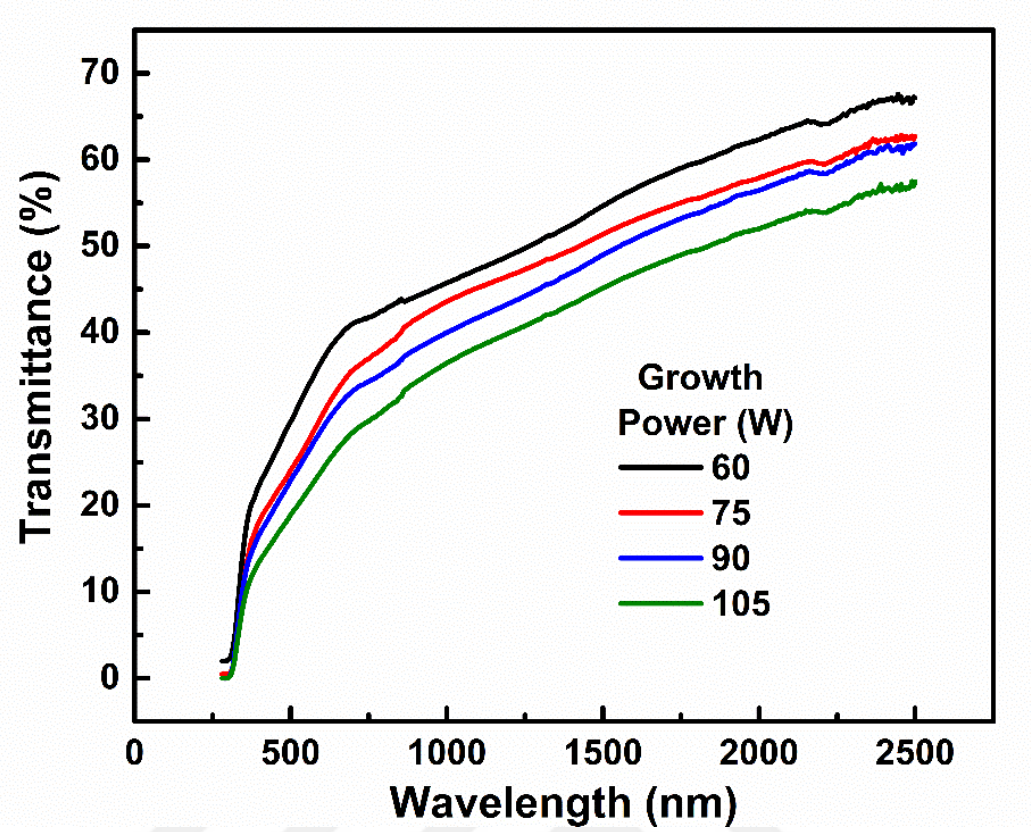

Figure 6.9: The optical transmittance spectrum of as-deposited NiO films deposited on ITO/Glass substrate at various growth powers.

The crystalline structures of NiO films were confirmed by XRD. Figure 6.10 shows the XRD patterns of ITO/glass substrate and NiO films deposited on ITO/glass substrates at different growth powers.

For NiO film deposited at 10 mTorr growth pressure, besides peaks associated with ITO structure, there are three diffraction peaks observed at approximately 36.5°, 42.1° and 62.2°, along (111), (200), and (220) planes, corresponding to a cubic NiO phase (JCPDS 22-1189). Generally, (111) plane can be more densely packed atoms with NiO thin film due to its higher intensity than the other planes of (200) and (220).

The peak positions slightly shifted a lower angle with increasing sputtering power when XRD patterns were examined in detail. The 2θ position of the preffered (111) oriantation shifted from 36.92° to 36.72° and (200) oriantation shifted from 42.72° to 42.62° as the growth power gradually increased. The shifting of the peaks could be ascribed to the presence of the lattice strain in the film.

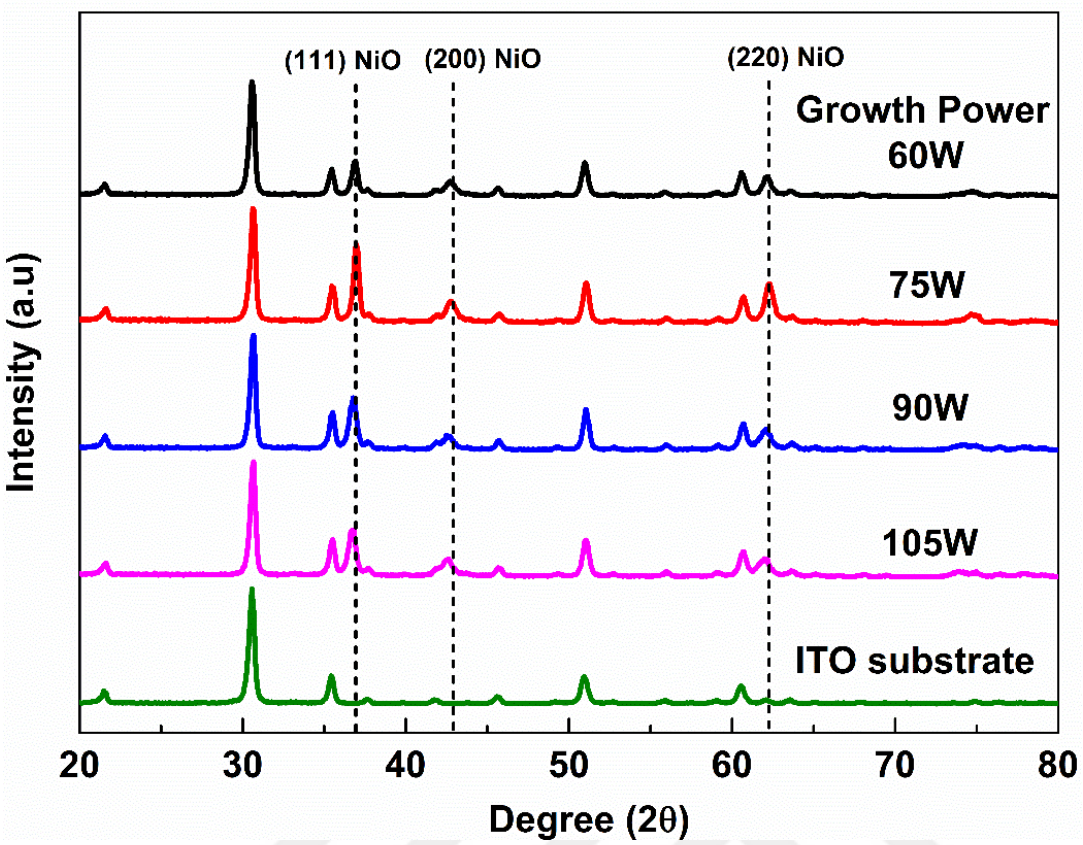

Figure 6.10: XRD patterns of ITO/glass substrate and as-deposited NiO films deposited on ITO/glass substrates at various growth powers.

The surface morphologies of NiO films were analyzed by AFM and SEM. Figure 6.11 shows the 2D AFM images of NiO films deposited at different growth powers, in the scan range of 3 µm x 3 µm. The grain size distribution is homogeneous for all films. These results indicate that increment in sputtering power from 60W to 105W would not ruin the homogeneity of films.

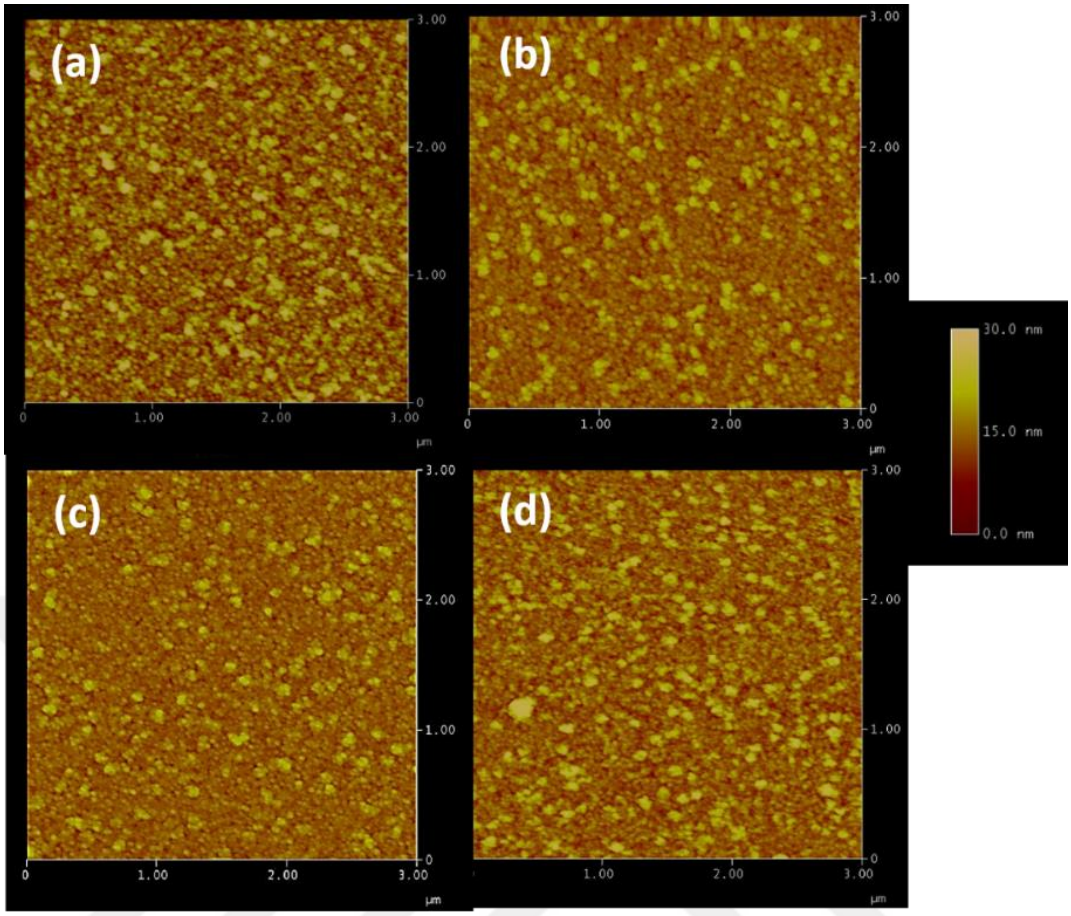

Figure 6.11: The two dimensional 3x3 µm AFM images of the NiO films deposited on ITO/glass substrates at various growth powers: (a) 60 W (b) 75 W (c) 90 W, and (d) 105 W.

The roughness values of NiO films were given in Table 6.5. The average surface roughnesses (Ra) are given in Table 6.5 which are 3.10, 3.31, 3.45, and 2.68 nm for the films deposited at growth powers of 60, 75, 90, and 105W, respectively Even though the film deposited at 90W has the highest roughness value, there is not an important difference between the roughness values.

Table 6.5: Roughness values of NiO films deposited on ITO/glass substrates at different growth powers.

Growth Power (W)	R_q (nm)
60	4.065
75	3.977
90	4.022
105	3.606

In figure 6.12, the plan view and cross-section SEM images of the films were presented. The scale bar of SEM images is 1 µm, scale bar of inset figures is 200 nm. The surface morphology of films has triangular features with linear extension as in the

previous set of experiments. The film surfaces are quite homogeneous. It has been understood that a power increase between 50W and 105W is not such an increase that will impair the surface homogeneity. Cross-section of the film deposited at 105 W shows film thickness is approximately 149 nm (in figure 6.12 (e)), it is very close to the measurement results of the profilometer.

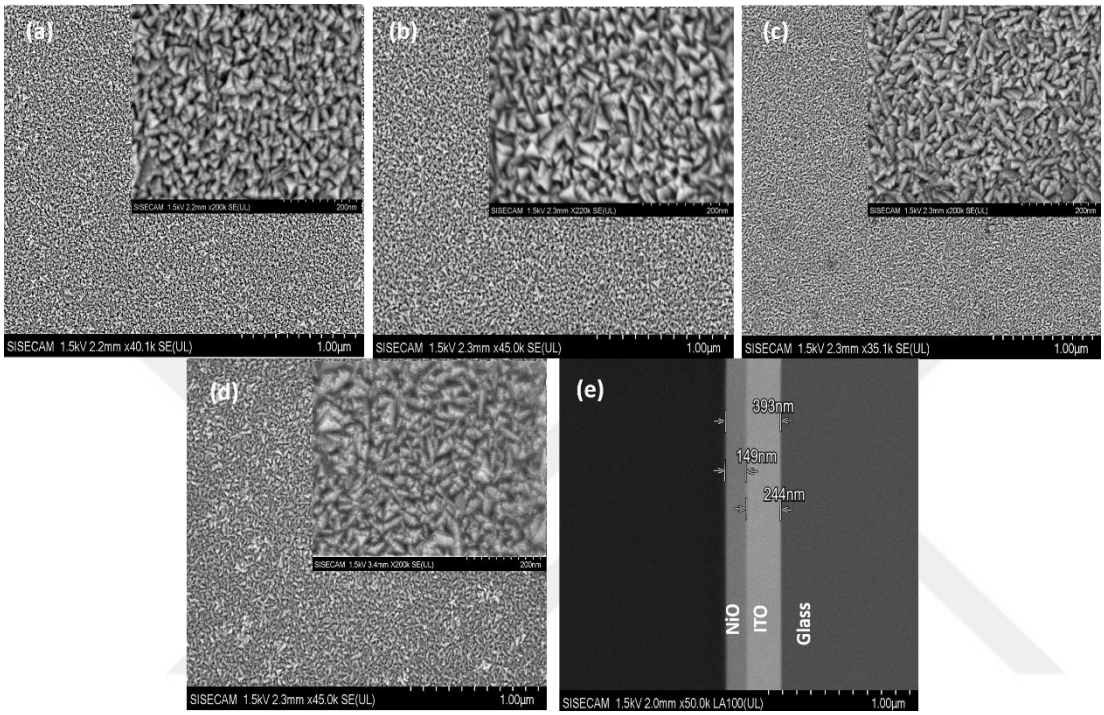

Figure 6.12: SEM images for the NiO films deposited on ITO/glass substrates at various growth powers: (a) 60 W (b) 75 W (c) 90 W (d) 105 W (e) cross-section SEM image for the NiO film deposited growth power of 105W.

CV was performed as same as mesurements in previous set of experiments. With the change in growth power from 60 W to 90 W, there is a rise in the current density values for both anodic and cathodic scans as given in figure 6.13. For the upper value of growth power than 90W, the current density values were decreased. The maximum cathodic and anodic currents were observed as 0.90 mA and -0.66 mA at 1.355 V and -0.325V for the 90W sample, respectively.

The results show that nickel oxide film deposited at 90W has the highest charge capacity.

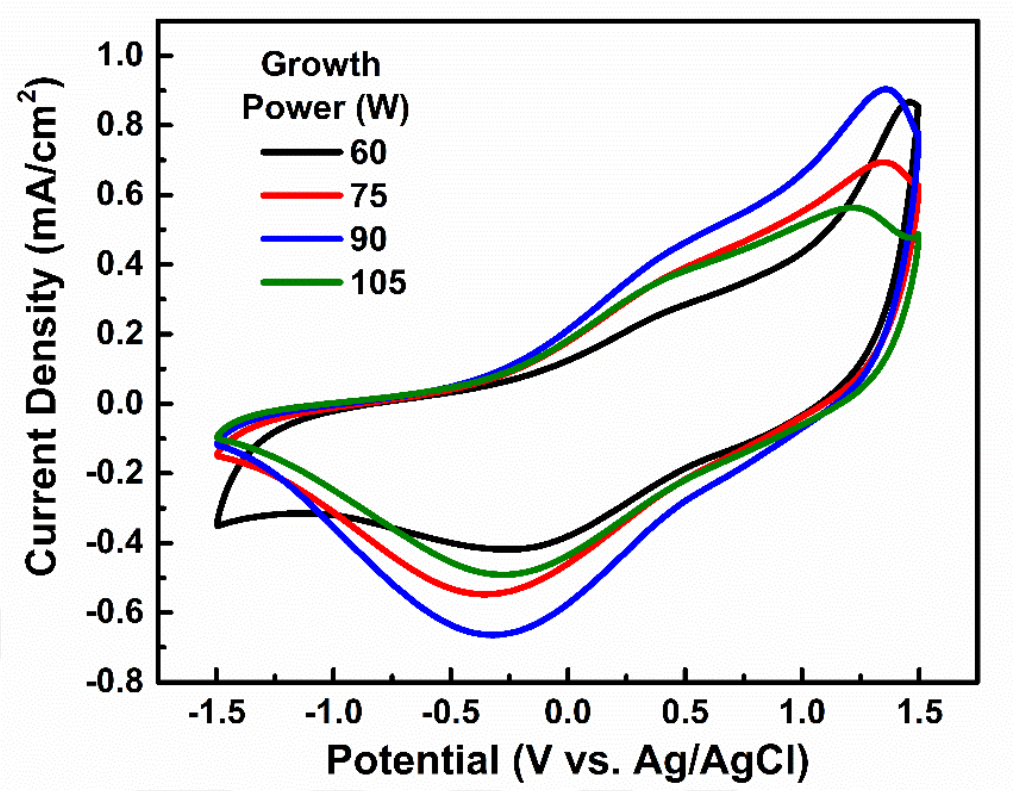

Figure 6.13: Cyclic voltammetry curves of NiO films deposited at various growth powers on ITO/glass substrates.

CA measurements were performed as same as mesurements in previous set of experiments. The in-situ transmittance of NiO films at a wavelength of 630nm was measured with CA, simultaneously.

Figure 6.14 shows the (a) CA curves, (b) in-situ transmittance results, and (c) optical modulations (at a constant wavelength of 630nm) of NiO films deposited with various growth powers. According to the measurement results, the amount of charges inserted/extracted to the film, response times, and optical densities of the films were computed and given in Table 6.6.

From the measurements in figure 6.14, the most bleached film was observed at 90 W. Also, this film has the highest optical modulation (43.4%). There is an increase in the amount of charges inserted/extracted to the films with increasing growth power up to 90W and then decreased with increasing growth power. This result shows similar behavior with CV.

The computed data in Table 6.6 indicate that the film deposited at 90W exhibited the highest transmittance (89.1%) in bleached state and the highest optical modulation

(43.4%) due to its high charge capacity. The optical modulation decrease with increasing growth power of more than 90W.

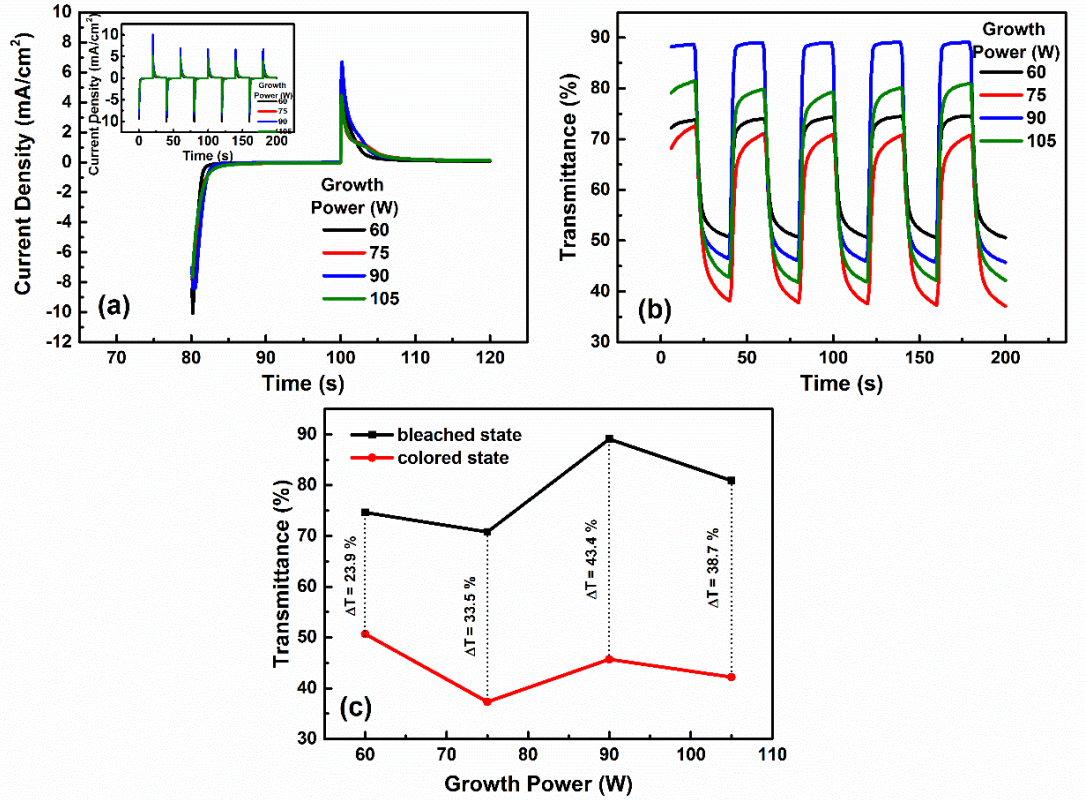

Figure 6.14: (a) Time response of the current density (Inset shows the plot of CA for 5 cycles) (b) in situ transmittance at 630 nm in five CA cycles **(c)** the bleached and colored state transmittances and optical modulations of NiO films deposited at various growth powers.

As we can see from the computed data in Table 6.6, bleaching is faster than coloration for all films. Since the inserted charge is higher than the extracted charge, it is necessary a shorter time to extract ions than insert them. The bleaching time is decreased from 8s to 4s with increasing growth power up to 90W and then increased from 4s to 9s with increasing growth power above 90W. The fastest bleaching and coloration process occurred for 90W growth power.

Table 6.6 also shows that the optical density gradually increases with an increase in growth power, and reached its maximum value of 0.67 at 90 W. With increasing growth power above 90 W, optical density started to decrease.

With ellipsometry measurements, we obtained refractive index (n) of as-deposited NiO films on glass. From the refractive indices of the films, corresponding surface porosity

values were calculated using equation 5.1. The density of films was determined from XRR results.

Table 6.6: The amount of charges inserted/extracted to the films, response times, and optical densities for bleaching and coloring processes of NiO films deposited at various growth powers.

Growth Power (W)	Q_{in} mC	Q_{out} mC	Bleaching Time (s)	Coloration Time (s)	Optical Density
60	9.941	8.832	6	10	0.36
75	10.463	9.616	8	10	0.64
90	13.307	11.501	4	8	0.67
105	10.099	9.378	9	10	0.65

With ellipsometry measurements, we obtained refractive index (n) of as-deposited NiO films on glass. From the refractive indices of the films, corresponding surface porosity values were calculated using equation 5.1. The density of films was determined from XRR results.

The change in the film density, refractive index (n), and surface porosity depending on growth power was presented in figure 6.15. A fluctuation was observed in refractive index, porosity, and density values with increasing growth power from 60W to 105W.

The refractive index of films was decreased from 1.98 to 1.88 and corresponding surface porosities were increased from 16.73% to 25.20% with increasing growth power from 60W to 75W. The maximum porosity value was observed for the film deposited at 75W. With increasing growth power from 75W to 105W, an increase in refractive index was observed, causing a decrease in porosity. And the change in film densities is not correlated with the change in porosity.

Although the film deposited at 75W had the highest porosity, the film coated at 90W showed the best electrochromic properties in terms of optical modulation, response time, and charge capacity.

As a result of the characterizations, it was decided to choose 90W growth power for the next experiments.

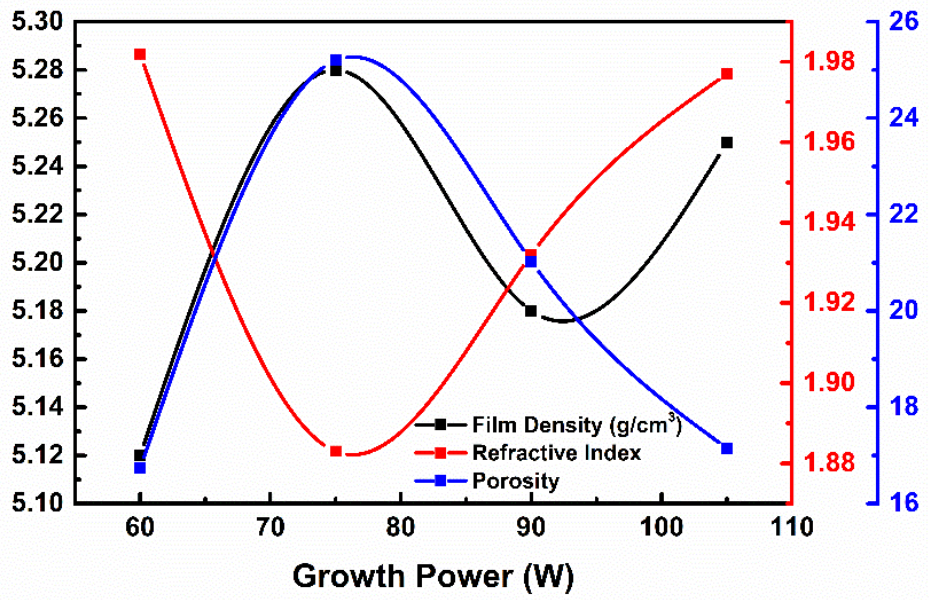

Figure 6.15: Film density, refractive index (at 630nm) and surface porosity of as-deposited NiO films on glass deposited at various growth powers.

6.3 Effect of the Growth Pressure on the Electrochromic Properties of NiO

In this section, thin films of Ni oxide were deposited by reactive radio frequency RF sputtering at 10, 13, 17, and 25 mTorr growth pressures (Ar working pressure), and their electrochromic properties were examined. The purpose of this set to clarify effects of RF growth pressure on the optical and electrochromic properties of NiO films and determine the most efficient growth pressure. The nickel oxide films were deposited on ITO films with 0.8 x 1.25 cm^2 and 16-17 Ω/sq sheet resistance. The power and oxygen content were individually kept at 90W and 90%. Film thicknesses were measured with the Dektak Vecoo profilometer. The coating parameters were presented in Table 6.7.

Table 6.7: Coating parameters of NiO films deposited at different growth powers.

Growth Pressure (mTorr)	Growth Power (W)	Working Pressure (Torr)	$Ar:O_2$ Ratio (%)	$Ar:O_2$ Ratio (sccm)	Rate (Å/s)	Thickness (nm)
10	90	$5.89x10^{-3}$	10 : 90	0.8 : 3.8	0.15	115
13	90	$1.12x10^{-2}$	10 : 90	1.1 : 4.7	0.27	155
17	90	$1.16x10^{-2}$	10 : 90	2.2 : 7.3	0.23	153
25	90	$1.75x10^{-2}$	10 : 90	3.0 : 10.5	0.19	110

The crystalline structures of NiO films were confirmed by X-Ray Diffraction (XRD) and given in figure 6.17. The graph shows the XRD patterns of ITO/glass substrate and NiO films deposited on ITO/glass substrates at different growth pressures. Except for peaks associated with ITO structure, there are three peaks observed around 36.9°, 42.7°, and 62.3°, along (111), (200), and (220) planes. These peaks are corresponding to a cubic NiO phase (JCPDS 22-1189). There is a shifting to higher values of diffraction angles with increasing growth power.

As observed in previous set of experiments, the growth pressure also changes the lattice strain.

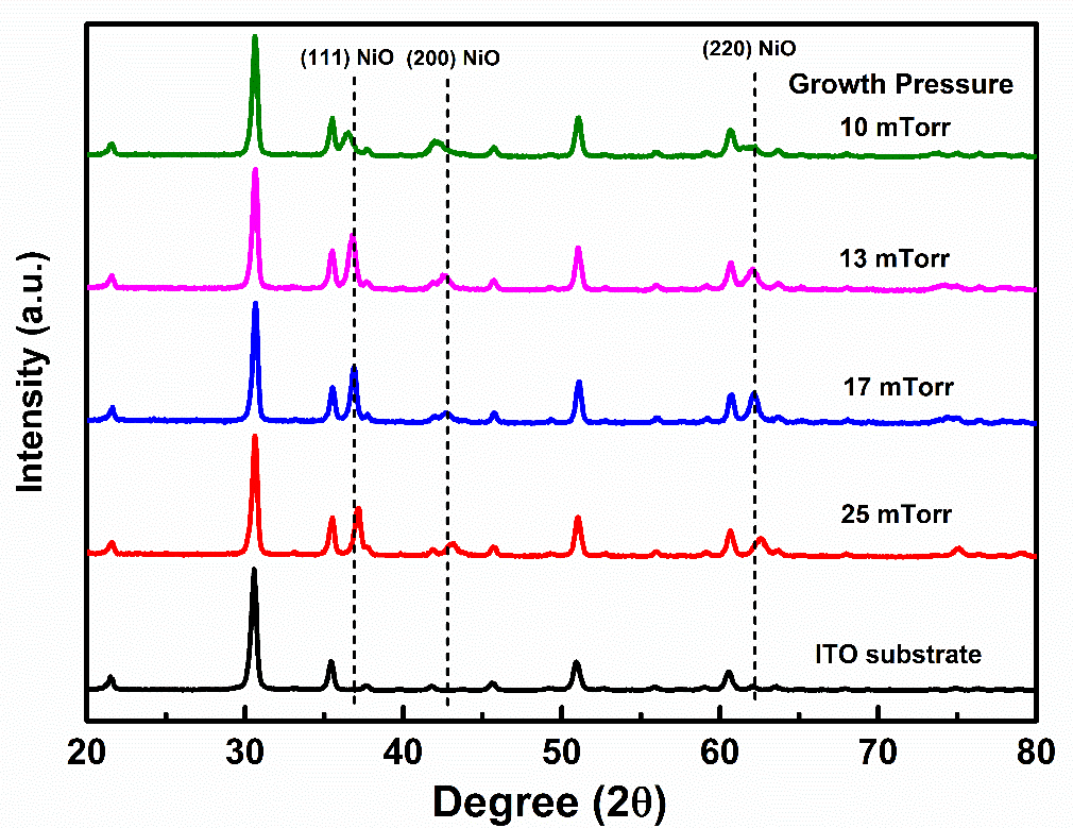

Figure 6.16: XRD patterns of ITO/glass substrate and as-deposited NiO films deposited on ITO/glass substrates at various growth pressures.

The surface morphologies of nickel oxide films were analyzed by AFM and FEGSEM. The 2D AFM images of NiO films deposited at different growth pressures are given in figure 6.18, in the scan range of 3 μm x 3 μm. AFM images in figure 6.18 show that more homogeneous grain size distribution the lowest grain size observed for the film deposited at 13mTorr growth pressure. There are agglomerated regions on the surface of nickel oxide films for depositions at other growth pressures.

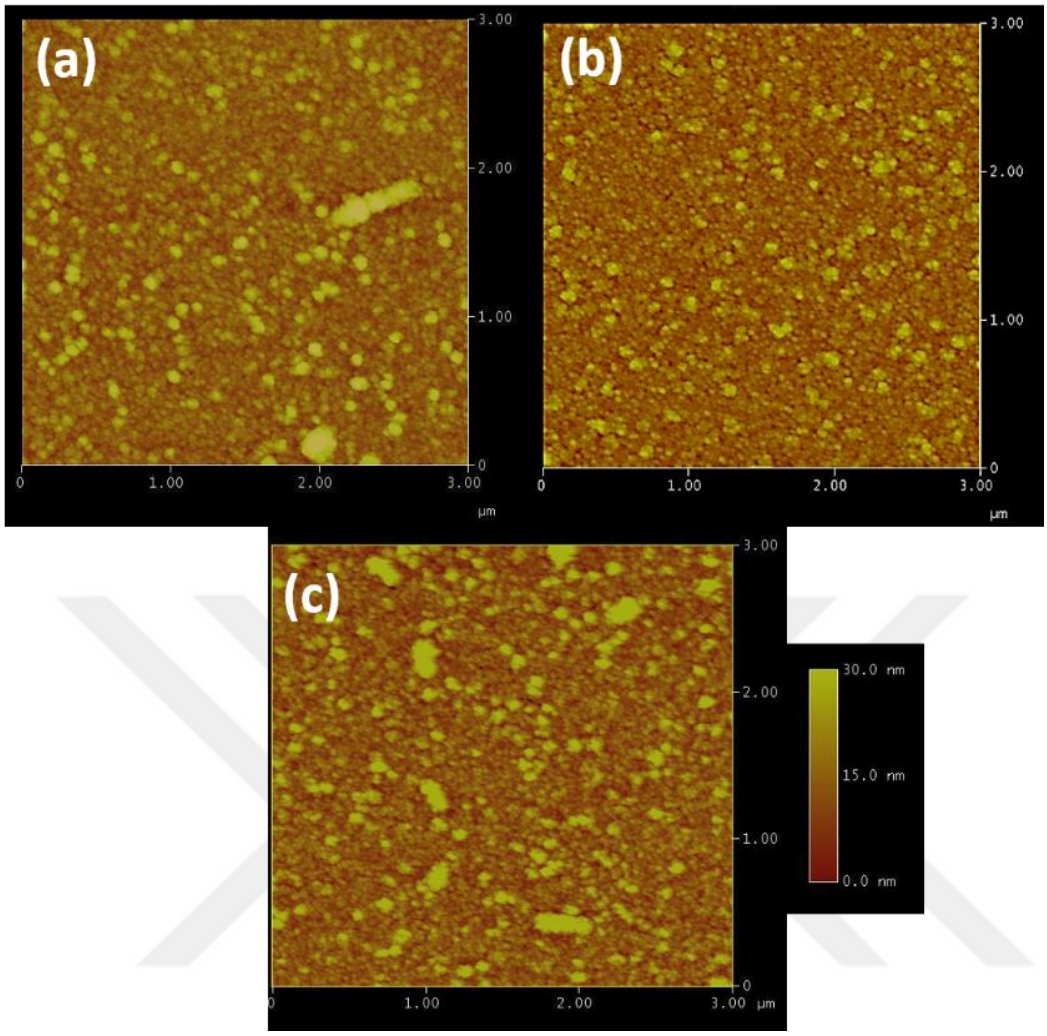

Figure 6.17: The two dimensional 3x3 µm AFM micrographs for the NiO films deposited on ITO/glass substrates at various growth pressures: (a) 10mTorr (b) 13mTorr (c) 25mTorr.

In figure 6.19, the plan-view SEM images of the NiO films were presented. The scale bar of SEM images is 1 µm, the scale bar of inset figures is 200nm. The surface of all samples was observed as quite homogeneous.

CV was performed as same as in the previous sets and given in figure 6.20. With the change in growth pressure from 10mTorr to 13mTorr, a significant rise was observed in the current density for both anodic and cathodic scans. For the upper value of growth pressure than 13mTorr, the current density values were decreased. The maximum cathodic and anodic currents were observed as 0.90 mA and -0.66 mA at 1.355 V and -0.325V for the 13mTorr sample, respectively. The CV results show that nickel oxide film deposited at 13mTorr has highest charge capacity.

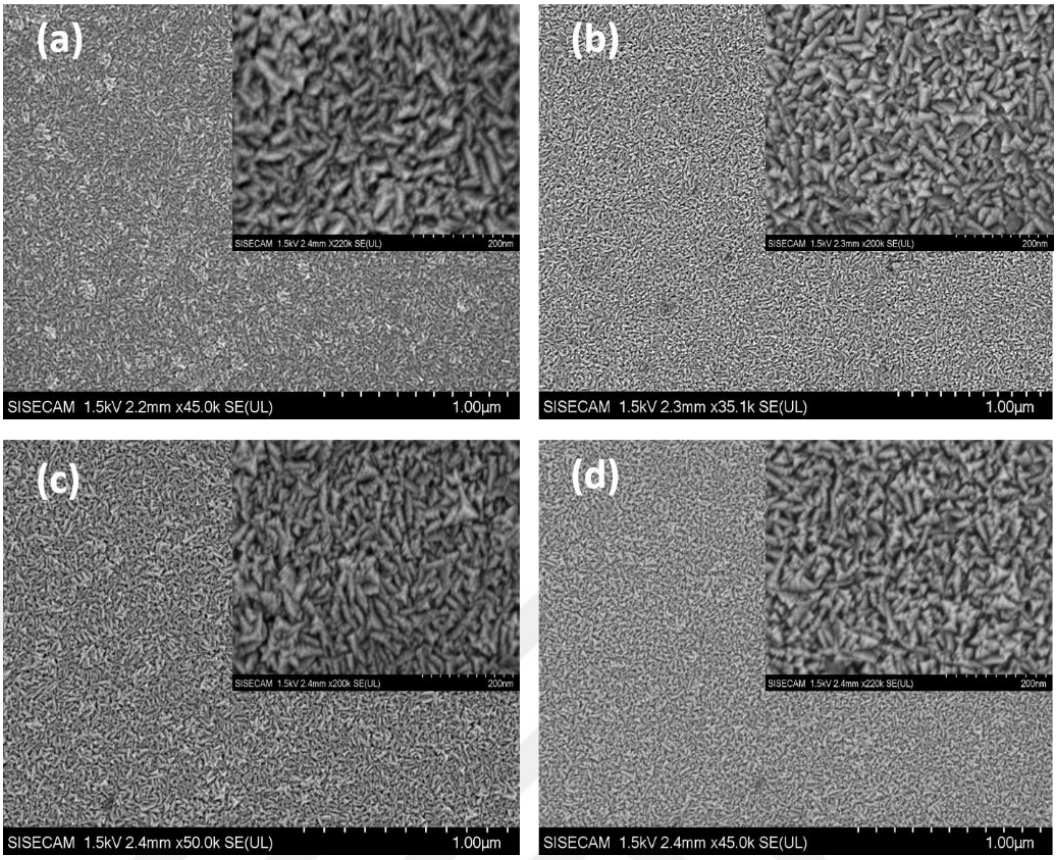

Figure 6.18: SEM images for the NiO films deposited on ITO/glass substrates at various growth pressures: ((a) 10 mTorr (b) 13 mTorr (c) 17 mTorr (d) 25 mTorr.

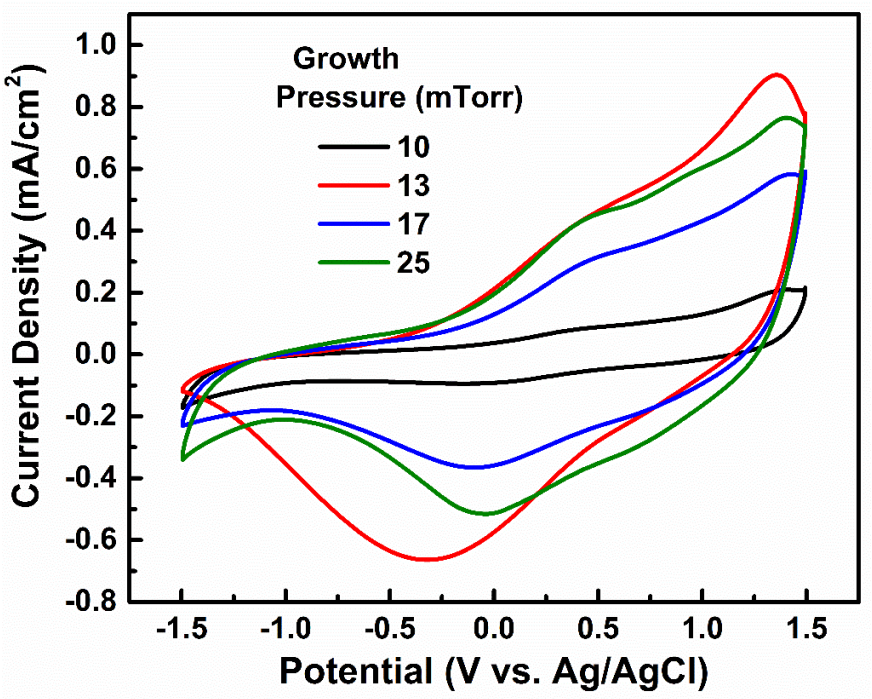

Figure 6.19: Cyclic voltammetry curves of NiO films deposited at various growth pressures on ITO/glass substrates.

CA measurements were performed as same as mesurements in previous set of experiments. The in-situ transmittance of films at a wavelength of 630nm was measured with CA, simultaneously. Figure 6.21 shows the (a) CA curves, (b) in-situ transmittance results (c) optical modulation values, and (d) optical density and coloration efficiency values (at a constant wavelength of 630nm) of NiO films deposited at various growth pressures. From the measurements in figure 6.21 (b), the most bleached film (89.1%) was observed for the film deposited at 13 mTorr growth pressure. Also, the film deposited at 13mTorr has the highest optical modulation (43.4%). An increase in optical modulation was observed with increasing growth pressure until 13mTorr. Then, the optical modulation values were decreased with increasing upper values of growth pressures. The increment in colored state transmittance from 46.3% to 60.5% was observed. Depending on these results, a similar change was observed in optical density and coloring efficiency values. The highest optical density and coloration efficiency were observed as 0.67 and 50.17 cm^2/mC at 13 mTorr growth pressure, respectively.

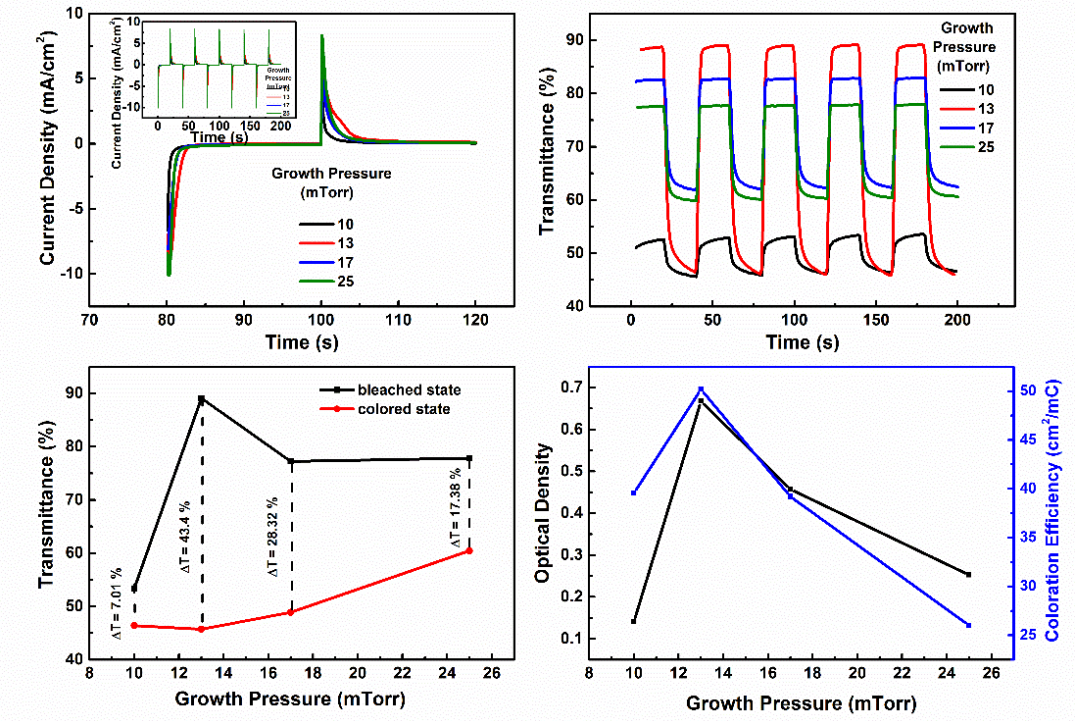

Figure 6.20: (a) Time response of the current density (Inset shows the plot of CA for 5 cycles) (b) in situ transmittance at 630 nm in five CA cycles (c) the bleached and colored state transmittances and optical modulations (d) optical density and coloration efficiency values of NiO films deposited at various growth pressures.

According to the measurement results, the amount of charges inserted/extracted to the film and response times of the films were computed and given in Table 6.7. There is an increase in the amount of charges inserted/extracted to the films with increasing growth pressure up to 13mTorr and then decreased with increasing growth pressure. This result shows similar behavior with CV experiments and shows that the 13mTorr sample has the highest charge capacity.

The computed data in Table 6.8 indicate that the film deposited at 13mTorr exhibited the highest transmittance (89.1%) in the bleached state, highest optical modulation (43.4%). There is continuous improvement in response times for coloring and bleaching processes with increasing growth pressure. The fastest bleaching and coloration process occurred for the NiO film deposited at 25mTorr as 2s and 5s, respectively. Although the response time improved with increasing growth pressure, the electrochromic properties of NiO films deteriorated above the 13mTorr. Response time alone is not sufficient to determine the film with the best electrochromic properties.

Table 6.8: The amount of charges inserted/extracted to the films, response times for bleaching and coloring processes of NiO films deposited at various growth pressures.

Growth Pressure (W)	Q_{in} mC	Q_{out} mC	Bleaching Time (s)	Coloration Time (s)
10	3.558	8.832	6	11
13	13.307	11.501	4	8
17	12.565	11.638	3	6
25	7.499	7.215	2	5

Following spectroscopic ellipsometry measurements, we obtained the refractive index (n) of as-deposited NiO films on glass. From the refractive index values of the films, corresponding surface porosity values were calculated using equation 5.1.The change in refractive index (n) and surface porosity depending on the growth pressure was presented in figure 6.22. A fluctuation was observed in the refractive index, porosity, and density values with increasing growth pressure from 10mTorr to 25mTorr. The refractive indices of films was decreased from 2.05 to 1.93 and corresponding surface porosities were increased from 10.76% to 21% with increasing growth pressure from 10mTorr to 13mTorr. The maximum porosity value was observed for the film deposited at 13mTorr. The decrease in porosity shows that an increase in film density.

Since the film is dense, the ions diffuse over very short distances. Therefore, a decrease in response time is a reasonable result.

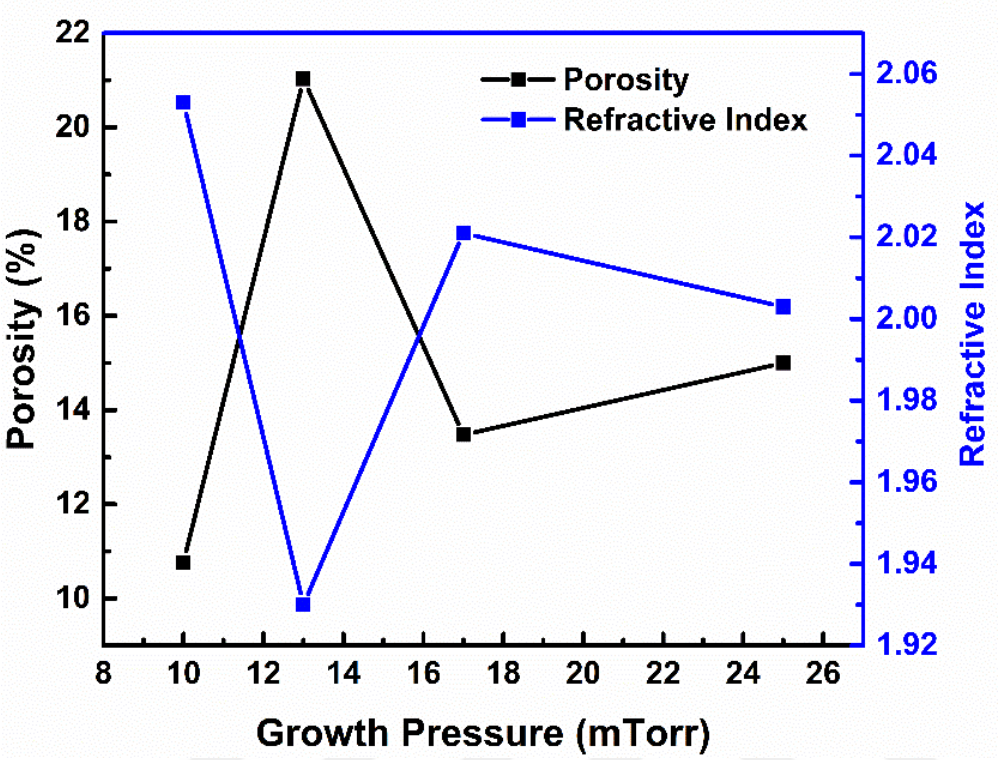

Figure 6.21: Refractive index (at 630nm) and surface porosity of as-deposited NiO films on glass deposited at various growth pressures.

It was determined that the optimized sputtering parameters of nickel oxide thin films with maximum electrochromic performance were 90% oxygen content, 90W growth power and 13mTorr growth pressure.

7. CONCLUSION

In this thesis study, nickel oxide films were deposited by RF magnetron sputtering from nickel metal target with different sputtering parameters. The purpose of the study to determine the effect of sputtering conditions on electrochromic properties of nickel oxide thin films. From the structural, morphological, and electrochemical measurements of the films, the effect of sputtering parameters on the electrochromic properties of NiO films was investigated. In the first set of experiments, the film deposited on ITO/glass substrates with various oxygen partial pressures (oxygen content O_2/O_2+Ar % in the sputtering atmosphere) of 50, 60, 70, and 90%. The electrochromic properties of NiO films were investigated by keeping the growth power and pressure constant as 60W and 13mTorr, respectively. From the structural, morphological, and electrochemical measurements of the films, the increased oxygen content in the sputtering atmosphere leads to the improvement of the electrochromic properties of films. Based on the XRD results, the change in oxygen content did not cause a change in the structural properties of the films. From SEM measurements increasing oxygen content from 50% to 90%, the surface morphology of the films has become more homogeneous and the grain sizes were decreased. From the electrochemical measurements, it has been determined that the increased amount of oxygen causes an increase in the charge capacity of the film due to an increase in porosity from 15.49% to 27.68%. And also, a decrease in the film density from 5.33 to 5.11 was determined from XRR measurements. It was determined that the film deposited with 90% oxygen content has high charge capacity, high optical modulation (23.9%), and fast response time (6s for coloration and 10s for bleaching process) due to its improved porosity which is made easy to ion insertion of the film matrix. With the examination of all characterizations, the 90% oxygen content was chosen for the next experiments.

In the second set of experiments, with choosing the oxygen content, NiO films deposited on ITO/glass substrates with various RF magnetron sputtering growth powers of 60W, 75W, 90W, and 105W. The films were deposited by keeping the

oxygen content in the sputtering atmosphere and growth pressure constant as 90% and 13mTorr, respectively. The XRD results show that the crystal structure of NiO films did not change with the change of growth power. The distribution of grain size is more homogeneous for the film deposited at 90W based on AFM images. In addition, the surface of the films became ununiform at higher growth powers than 90 W. It is indicated that excessive sputtering power would destroy the integrality of the films and can cause particle agglomeration on the surface. Quite homogeneous surfaces were observed in SEM images, but as observed in the AFM images, the film with the most homogeneous surface is the film deposited at 90W growth power. In addition to these results, the highest current density, which means that the high charge capacity of the films, was observed for the 90 W growth power from the CV measurement. All of these results correlated with the chronoamperometry and transmittance-time measurement results. The calculated amount of charges inserted/extracted into/out the NiO films from CA curves were increased up to 90W growth power and then decreased with increasing growth power above 90W. The film deposited at 90 W has the highest optical modulation (43.4%), response times (4s for bleaching and 8s for coloration process), and optical density (0.67). Although the film deposited at 75W growth power had the highest porosity, NiO thin film coated at 90W showed the best electrochromic properties in terms of optical modulation, response time, and charge capacity. For this reason, as a result of the characterizations, it was decided to choose 90W growth power for the next experiments.

In the third set of experiments, the films deposited on ITO/glass substrates with various growth pressures of 10, 13, 17, and 25mTorr by keeping the oxygen content and growth power constant as 90% and 90W, respectively. The effect of increasing growth pressure on the electrochromic properties of NiO films was investigated by the structural, morphological, and electrochemical measurements. The crystal structure of the NiO films did not change with the change of growth pressure. AFM and SEM images show that the distribution of grain size is more homogeneous for NiO film deposited at 13mTorr. From the SEM images, the lowest grain size observed for the film deposited at 13mTorr growth pressure. In addition to these results, the electrochemical measurements were performed. The current densities were increased up to 13mTorr growth pressure and then decreased with increasing growth pressure above 13mTorr. And also, the film deposited at 13mTorr has the highest optical

modulation (43.4%) and highest coloration efficiency (50.17 cm^2/mC). There is continuous improvement in response times for coloring and bleaching processes with increasing growth pressure. The fastest bleaching and coloration process occurred for the NiO film deposited at 25mTorr as 2s and 5s, respectively. According to the ellipsometry measurement results, the most porous film is the film deposited at 13 mTorr. In addition, it can be say that, this film has lowest film density due to the decrease in porosity shows that an increase in film density. Since the film is dense, the ions diffuse over very short distances. Therefore, a decreased in response time with increasing pressure can be a reasonable result. From this set of experiments, it was concluded that the film deposited at 13mTorr growth pressure has the best electrochromic properties. At the end of the study, it was determined that the optimized sputtering parameters of nickel oxide thin films with maximum electrochromic performance were 90% oxygen content, 90W growth power, and 13mTorr growth pressure.

As a result of this thesis study, the sputtering parameters as oxygen content in the sputtering atmosphere, growth power, and pressure were optimized to determine which NiO films have the best electrochromic properties. The determined sputtering parameters are 90 % oxygen content, 90 W growth power, and 13 mTorr growth pressure. For all sets of experiments, the thicknesses of films were tried to be constant to avoid the thickness effect on electrochromic properties. This thesis has the efficient results to show the importance of RF magnetron sputtering deposition parameters on the electrochrochromic properties of NiO films. According to these parameters, the effect of varying porosity on the electrochromic properties of NiO thin films is discussed. This thesis has contributed to the literature in determining the effect of RF magnetron sputtering parameters on the electrochromic properties of nickel oxide thin films due to surface porosity.

REFERENCES

[1] **L. Itard**, (2012). Energy in the built environment. *Sustainable Urban Environments*, 113-175

[2] **R. Baetens, B. P. Jelle, and A. Gustavsen**, (2010). Properties, requirements and possibilities of smart windows for dynamic daylight and solar energy control in buildings: A state-of-the-art review, *Solar Energy Materials and Solar Cells*. 94(2), 87-105.

[3] **C. G. Granqvist**, "Handbook of Inorganic Electrochromic Materials."

[4] **C. G. Granqvist, E. Avendaño, and A. Azens,** (2003). Electrochromic coatings and devices: Survey of some recent advances, 442(1-2), 201-211.

[5] **K. A. Gesheva, T. M. Ivanova, and G. Bodurov**, (2012). Transition metal oxide films: Technology and 'smart Windows' electrochromic device performance, 74(4), 635-639.

[6] **C.-Y. Chang and M.-K. Lee**, (2009) Electrochromic Properties of Tungsten Oxide Films Prepared by RF Sputtering and Liquid Phase Deposition,

[7] **J. W. Lim, S. J. Yoo, S. H. Park, S. U. Yun, and Y. E. Sung,** (2009) High electrochromic performance of co-sputtered vanadium-titanium oxide as a counter electrode, *Solar Energy Materials and Solar Cells*, 93(12), 2069-2074.

[8] **R. Sivakumar, C. S. Gopinath, M. Jayachandran, and C. Sanjeeviraja,** (2007). An electrochromic device (ECD) cell characterization on electron beam evaporated MoO3films by intercalating/deintercalating the H+ions, *Current Applied Physics*, 7(1), 76-86

[9] **S. Green, J. Backholm, P. Georén, C. G. Granqvist, and G. A. Niklasson**, (2009). Electrochromism in nickel oxide and tungsten oxide thin films: Ion intercalation from different electrolytes, *Solar Energy Materials and Solar Cells*, 93(12), 2050-2055.

[10] **H. Huang *et al.*,** (2011). Electrochromic properties of porous NiO thin film as a counter electrode for NiO/WO3complementary electrochromic window, *Electrochimica Acta*, 56(11), 4284-4286.

[11] **A. Urbano, F. F. Ferreira, S. C. DeCastro, R. Landers, M. C. A. Fantini, and A. Gorenstein,** (2001). Electrochromism in lithiated nickel

oxide films deposited by rf sputtering, *Electrochimica Acta*, 46(13-14), 2269-2273.

[12] **S. H. Park, J. W. Lim, S. J. Yoo, I. Y. Cha, and Y. E. Sung,** (2012). The improving electrochromic performance of nickel oxide film using aqueous N,N-dimethylaminoethanol solution, *Solar Energy Materials and Solar Cells*, 99, 31–37.

[13] **D. T. Gillaspie, R. C. Tenent, and A. C. Dillon,** (2010). Metal-oxide films for electrochromic applications: Present technology and future directions, *Journal of Materials Chemistry*, 43, 2010.

[14] **Z. Jiao, M. Wu, Z. Qin, and H. Xu,** (2003). The electrochromic characteristics of sol-gel-prepared NiO thin film, *Nanotechnology*, 14(4), 458–461.

[15] **A. C. Sonavane, A. I. Inamdar, P. S. Shinde, H. P. Deshmukh, R. S. Patil, and P. S. Patil,** (2009). Efficient electrochromic nickel oxide thin films by electrodeposition, *Journal of Alloys and Compounds*, 489(2), 667–673.

[16] **M. Z. Sialvi *et al.*,** (2013). Electrochromic and colorimetric properties of nickel(II) oxide thin films prepared by aerosol-assisted chemical vapor deposition, *ACS Applied Materials and Interfaces*, 5(12), 5675–5682.

[17] **H. Liu, W. Zheng, X. Yan, and B. Feng,** (2008). Studies on electrochromic properties of nickel oxide thin films prepared by reactive sputtering," *Journal of Alloys and Compounds*, 462, (1–2), 356–361.

[18] **J. D. Hwang and T. H. Ho,** (2017). Effects of oxygen content on the structural, optical, and electrical properties of NiO films fabricated by radio-frequency magnetron sputtering, *Materials Science in Semiconductor Processing*, 71, 396–400.

[19] **W. J. Lee *et al.*, (**2000). Effects of surface porosity on tungsten trioxide (WO3) films electrochromic performance, *Journal of Electronic Materials*, 29(2), 183–187.

[20] **Y. C. Nah,** (2011). Effects of sputter parameters on electrochromic properties of tungsten oxide thin films grown by RF sputtering," *Korean Journal of Materials Research*, 21(12) , 703–707.

[21] **P. Ashrit,** Transition metal oxide thin film-based chromogenics and devices.

[22] **E. M. Baba, J. Montero, E. Strugovshchikov, E. Ö. Zayim, and S. Karazhanov,** (2020). Light-induced breathing in photochromic yttrium oxyhydrides, *Physical Review Materials*, 4(2).

[23] **R. H. Mitchell,** (1999). The metacyclophanediene-dihydropyrene photochromic π switch, *European Journal of Organic Chemistry*, 11, 2695–2703.

[24] **M. M. Seyfouri and R. Binions,** (2017). Sol-gel approaches to thermochromic vanadium dioxide coating for smart glazing application, *Solar Energy Materials and Solar Cells*, 159, 52–65.

[25] **Y. Li, S. Ji, Y. Gao, H. Luo, and M. Kanehira,** (2013). Core-shell VO2 @TiO2 nanorods that combine thermochromic and photocatalytic properties for application as energy-saving smart coatings, *Scientific Reports*, 3, 1–13.

[26] **Z. Zhang *et al.*,** (2010). Thermochromic VO2 thin films: Solution-based processing, improved optical properties, and lowered phase transformation temperature, *Langmuir*, 26(13), 10738–10744.

[27] **S. M. Wang, L. Liu, W. L. Chen, and E. B. Wang,** (2013). High performance visible and near-infrared region electrochromic smart windows based on the different structures of polyoxometalates, *Electrochimica Acta*, 113, 240–247.

[28] **C. G. Granqvist, M. A. Arvizu, Bayrak Pehlivan, H. Y. Qu, R. T. Wen, and G. A. Niklasson,** (2018). Electrochromic materials and devices for energy efficiency and human comfort in buildings: A critical review, *Electrochimica Acta*, 259, 1170–1182.

[29] **M. Irie,** *Diarylethenes for Memories and Switches*, 100(5), 2000.

[30] **M. Bourdin *et al.*,** (2010). Investigation on the coloring and bleaching processes of WO3-: Xphotochromic thin films, *Journal of Materials Chemistry C*, 8(27), 9410–9421, Jul. 2020.

[31] **P. Jittiarporn, L. Sikong, K. Kooptarnond, and W. Taweepreda,** (2014). Effects of precipitation temperature on the photochromic properties of h-MoO3, *Ceramics International*, 40(8) PART B, 13487–13495.

[32] **Chennupati Jagadish, Stephen J. Pearton** – (2006). Zinc Oxide Bulk, Thin Films and Nanostructures_ Processing, Properties, and Applications-Elsevier Science.

[33] **R. Eglitis *et al.*,** (2020). Strong, Rapid, and Reversible Photochromic Response of Nb Doped TiO2Nanocrystal Colloids in Hole Scavenging Media," *ACS Applied Materials and Interfaces*, 12(51), 57609–57618.

[34] **S. Y. Lee, H. Lee, I. In, and S. Y. Park,** (2010). PH/redox/photo responsive polymeric micelle via boronate ester and disulfide bonds with

spiropyran-based photochromic polymer for cell imaging and anticancer drug delivery," *European Polymer Journal*, 57, 1–10.

[35] **Y. Huang, F. Li, C. Ye, M. Qin, W. Ran, and Y. Song,** (2015). A Photochromic Sensor Microchip for High-performance Multiplex Metal Ions Detection, *Scientific Reports*, 5, Apr.

[36] **H. Tian and Y. Feng,** (2008). Next step of photochromic switches, *Journal of Materials Chemistry*, 18(14), 1617–1622.

[37] **L. Liu, S. Peng, W. Wen, and P. Sheng,** (2007). Paperlike thermochromic display, *Applied Physics Letters*, 90(21), 213508.

[38] **G. Kim *et al.*,** (2017). Pressure-Mapped Thermochromic Interactive Sensor, *Advanced Materials*, 29(13).

[39] **G. Lee *et al.*,** (2020). User-Interactive Thermotherapeutic Electronic Skin Based on Stretchable Thermochromic Strain Sensor, *Advanced Science*, 7(17).

[40] **P. Talvenmaa,** (2006). "Introduction to chromic materials," 193–205.

[41] **R. R. Chance, R. H. Baughman, H. Müller, and C. J. Eckhardt,** (1977). Thermochromism in a polydiacetylene crystal," *The Journal of Chemical Physics*, 67(8), 3616–3618.

[42] **O. Ingan, W. R. Salaneck, J.-E. Osterholm, and J. Laakso,** (1998). THERMOCHROMIC AND SOLVATOCHROMIC EFFECTS IN POLY(3-HEXYLTHIOPHENE, *Synthetic Metals*, 22(4), 395-406.

[43] **C.-H. Yuan and R. West,** (1998). Amorphous Poly[(alkoxy-n-alkyl)methylsilane]s and Crystalline Poly[bis(alkoxy-n-alkyl)silane]s: The Effect of Side-Chain Flexibility on the Thermochromic Transition, 1998. [Online]. Available: https://pubs.acs.org/sharingguidelines

[44] **Cehiao et al.** (1988). Alkoxy-Substituted Poly(diarylsilanes): Thermochromism and Solvatochromism , *Macromolecules,* 21, 3120-3122.

[45] **N. R. Mlyuka, G. A. Niklasson, and C. G. Granqvist,** (2009). Thermochromic multilayer films of VO2 and TiO2 with enhanced transmittance, *Solar Energy Materials and Solar Cells*, 93(9), 1685–1687.

[46] **G. Jorgenson,** Lawrence Berkeley National Laboratory Recent Work Title ELECTROCHROMATIC AND THERMOCHROMIC MATERIALS FOR SOLAR ENERGY APPLICATIONS WITH EMPHASIS ON NIOBIUM AND VANADIUM OXIDES

Permalink Publication Date. [Online]. Available: https://escholarship.org/uc/item/9nr3b8ww

[47] **Y. Nah, K. Ahn, and Y. Sung,** "Effects of tantalum oxide films on stability and optical memory in electrochromic tungsten oxide films Effects of tantalum oxide films on stability and optical memory in electrochromic tungsten oxide films, *Solid State Ionics*, 165(1-4), 229-233.

[48] **P. Andersson, R. Forchheimer, P. Tehrani, and M. Berggren,** (2007). Printable all-organic electrochromic active-matrix displays, *Advanced Functional Materials*, 17(16), 3074–3082.

[49] **B. Seung *et al.*,** (2005). Nanotube-Based Ultrafast Electrochromic Display, *Advanced Materials*, 2, 171–175.

[50] **F. G. K. Baucke,** (1991). Electrochromic applications, 1, 285–292.

[51] **F. Mesoporous *et al.*,** (2003). Enhancement of Photocatalytic and Electrochromic Properties of Electrochemically, *Advanced Materials*, 15(15), 1269–1273.

[52] **K. K. Purushothaman and G. Muralidharan,** (2011). Enhanced electrochromic performance of nanoporous NiO films, *Materials Science in Semiconductor Processing*, 257(7), 2647-2656.

[53] **I. Mjejri, M. Gaudon, and A. Rougier,** (2019). Mo addition for improved electrochromic properties of V2O5 thick films, *Solar Energy Materials and Solar Cells*, 198, 19–25.

[54] **L. Ottaviano, A. Pennisi, F. Simone, and A. M. Salvi,** (2004). RF sputtered electrochromic V2O5 films, *Optical Materials*, 27(2), 307-313.

[55] **A. A. Æ. C. G. Granqvist,** (2003). Electrochromic smart windows : energy efficiency and device aspects, *Journal of Solid State Electrochemistry*. 7, 64–68.

[56] **P. Camurlu,** (2014). Polypyrrole derivatives for electrochromic applications," *RSC Advances*, 4(99), 55832–55845.

[57] **T. Jiemsakul, K. Jiramitmongkon, U. Asawapirom, and C. Chotsuwan,** (2017). Investigation of P3HT electrochromic polymer films prepared by ultrasonication of polymer solutions, *Journal of Materials Science*, 52, 7485-8492.

[58] **M. F. Zainal, Y. Mohd, and R. Ibrahim,** (2013). Preparation and characterization of electrochromic polyaniline (PANi) thin films, *BEIAC 2013 IEEE Business Engineering and Industrial Applications Colloquium*, 64–68.

[59] **J. Kawahara, P. A. Ersman, I. Engquist, and M. Berggren,** (2012). Improving the color switch contrast in PEDOT:PSS-based electrochromic displays, *Organic Electronics*, 13(3), 469–474.

[60] **M. D. Ward,** (2005). Near-infrared electrochromic materials for optical attenuation based on transition-metal coordination complexes,778–787.

[61] **T. L. Rose, S. D. Antonio, M. H. Jillson, A. B. Kon, R. Suresh, and F. Wang,** (1997). A microwave shutter using conductive polymers, *Synthetic Metals*, 85, 1439–1440.

[62] **D. P. Dubal, N. R. Chodankar, D. H. Kim, and P. Gomez-Romero,** (2018). Towards flexible solid-state supercapacitors for smart and wearable electronics," *Chemical Society Reviews*, 47(6), 2065–2129.

[63] **S. Santiago-Malagón, D. Río-Colín, H. Azizkhani, M. Aller-Pellitero, G. Guirado, and F. J. del Campo,** (2020). A self-powered skin-patch electrochromic biosensor," *Biosensors and Bioelectronics*, 175, 1–9.

[64] **C. M. Wang, C. Y. Wen, Y. C. Chen, S. Y. Lin, and S. T. Shiau,** (2013). Electrochromic property of sputtered amorphous NiO films, *Advanced Materials Research*, 693, 1685–1689.

[65] **C.-C. Chan *et al.*,** (2010). Electrochromic device with GZO as a conductive layer, *Current Developments in Lens Design and Optical Engineering XI; and Advances in Thin Film Coatings VI*, 7786, 77860S, 2010.

[66] **R. Sivakumar, R. Gopalakrishnan, M. Jayachandran, and C. Sanjeeviraja,** (2006). Investigation of x-ray photoelectron spectroscopic (XPS), cyclic voltammetric analyses of WO3 films and their electrochromic response in FTO/WO3/electrolyte/FTO cells, *Smart Materials and Structures*, 15(3), 877–888, 2006.

[67] **X. Jiang, F. L. Wong, M. K. Fung, and S. T. Lee,** (2003). Aluminum-doped zinc oxide films as transparent conductive electrode for organic light-emitting devices, *Applied Physics Letters*, 83(9), 1875–1877.

[68] **J. Y. Kim *et al.*,** (2018). Graphene electrode enabling electrochromic approaches for daylight-dimming applications, *Scientific Reports*, 8(1), 3944.

[69] **K. Y. Shen, C. W. Hu, L. C. Chang, and K. C. Ho,** (2011). A complementary electrochromic device based on carbon nanotubes/conducting polymers, *Solar Energy Materials and Solar Cells*, 98, 294–299.

[70] **J. Jensen, M. Hösel, I. Kim, J. S. Yu, J. Jo, and F. C. Krebs,** (2014). Fast switching ITO free Electrochromic devices, *Advanced Functional Materials*, 24(9), 1228–1233.

[71] **M. Jamdegni and A. Kaur,** (2020). Highly efficient dark to transparent electrochromic electrode with charge storing ability based on polyaniline and functionalized nickel oxide composite linked through a binding agent, *Electrochimica Acta*, 331, 135359, 2020.

[72] **S. Gottesfeld, J. D. E. McIntyre, G. Beni, and J. L. Shay,** (1978). Electrochromism in anodic iridium oxide films, *Applied Physics Letters*, 33(2), 208–210.

[73] **W. C. Dautremont-Smith,** (1982). Transition metal oxide electrochromic materials and displays: a review. Part 2: oxides with anodic coloration, *Displays*, 3(2), 67–80, 1982.

[74] **A. Georg, A. Georg, W. Graf, and V. Wittwer,** (2007). Switchable windows with tungsten oxide, *Vacuum*, 2008.

[75] **M. Ottaviani, S. Panero, S. Morzilli, B. Scrosati, and M. Lazzari,** (1986). The electrochromic characteristics of titanium oxide thin film electrodes, *Solid State Ionics*, 20(3), 197–202, 1986.

[76] **K. Yoshimura, T. Miki, S. Iwama, and S. Tanemura,** (1996). "Characterization of niobium oxide electrochromic thin films prepared by reactive d.c. magnetron sputtering, *Thin Solid Films*, 281–282(1–2), 235–238.

[77] **P. Cossari, C. Simari, A. Cannavale, G. Gigli, and I. Nicotera,** (2018). Advanced processing and characterization of Nafion electrolyte films for solid-state electrochromic devices fabricated at room temperature on single substrate,"*Solid State Ionics*, 317, 46–52, 2018.

[78] **J. H. Choy, Y. I. Kim, B. W. Kim, N. G. Park, G. Campet, and J. C. Grenier,** "New solution route to electrochromic poly(acrylic acid)/WO3 hybrid film," *Chemistry of Materials*, vol. 12, no. 10, pp. 2950–2956, 2000, doi: 10.1021/cm990718h.

[79] **O. Bohnke, C. Rousselot, P. A. Gillet, and C. Truche,** "Gel Electrolyte for Solid-State Electrochromic Cell," *Journal of The Electrochemical Society*, vol. 139, no. 7, pp. 1862–1865, 1992, doi: 10.1149/1.2069512.

[80] **D. Chimica, R. La, and A. Gorenstein,** "LixWOs/(PEO)sLiCIO4/NiO," no. 11, pp. 3394–3395, 1989.

[81] **R. B. Goldner *et al.*,** (1988). Thin film solid state ionic materials for electrochromic smart windowTM glass, *Solid State Ionics*, 28–30, PART 2, 1715–1721.

[82] **A. L. Larsson and G. A. Niklasson,** (2004). Infrared emittance modulation of all-thin-film electrochromic devices, *Materials Letters*, 2004.

[83] **C. Corbella, M. Vives, A. Pinyol, I. Porqueras, C. Person, and E. Bertran**, (2003). Influence of the porosity of RF sputtered Ta2O5 thin films on their optical properties for electrochromic applications, *Solid State Ionics*, 165(1), 15-22..

[84] **G. Vaivars, J. Kleperis, and A. Lusis,** (1993). Antimonic acid hydrate xerogels as proton electrolytes," *Solid State Ionics*, 61(4), 317–321.

[85] **Q. Liu, G. Dong, Y. Xiao, M. P. Delplancke-Ogletree, F. Reniers, and X. Diao,** (2016). Electrolytes-relevant cyclic durability of nickel oxide thin films as an ion-storage layer in an all-solid-state complementary electrochromic device, *Solar Energy Materials and Solar Cells*, 157, 844–852.

[86] **Y. Wang, J. Zhu, X. Yang, L. Lu, and X. Wang,** (2005). Preparation of NiO nanoparticles and their catalytic activity in the thermal decomposition of ammonium perchlorate, *Thermochimica Acta*, 437(1–2), 106–109.

[87] **K. S. Usha, R. Sivakumar, C. Sanjeeviraja, V. Sathe, V. Ganesan, and T. Y. Wang,** (2016). Improved electrochromic performance of a radio frequency magnetron sputtered NiO thin film with high optical switching speed," *RSC Advances*, 6(83), 79668–79680, 2016.

[88] **E. Avendaño, A. Azens, J. Isidorsson, R. Karmhag, G. A. Niklasson, and C. G. Granqvist,** (2003). Optimized nickel-oxide-based electrochromic thin films, *Solid State Ionics*, 165(1-4), 169-173.

[89] **W. L. Jang, Y. M. Lu, W. S. Hwang, T. L. Hsiung, and H. P. Wang,** (2009). Point defects in sputtered NiO films,"*Applied Physics Letters*, 94(6), 94–97, 2009.

[90] **H. Huang *et al.*,** (2011). v, *Electrochimica Acta*,

[91] **I. Bouessay, A. Rougier, P. Poizot, J. Moscovici, A. Michalowicz, and J. M. Tarascon,** "(2005). Electrochromic degradation in nickel oxide thin film: A self-discharge and dissolution phenomenon, *Electrochimica Acta*, 50(18), 3737–3745, 2005.

[92] **Y. G. Wu, G. M. Wu, X. Y. Ni, and X. Wu,** (2000). Ion transport in electrochromic nickel oxide thin films, *Solar Energy Materials and Solar Cells*, 63(2), 217–226, 2000,

[93] **Sara Green**, (2012), Electrochromic Nickel-Tungsten Oxides: Optical, Electrochemical and Structural Characterizations of Sputter-

Deposited Thin Films in the Whole Composition Range, *Uppsala University, Doctoral thesis.*

[94] **H. Frey and H. R. Khan,** *Handbook of Thin-Film Technology*. (2015).

[95] **P. D. Davidse,** (1967). Theory and practice of RF sputtering, *Microelectronics Reliability*, 6(4), 336.

[96] **M. M. Zagho, H. D. Dawoud, N. Bensalah, and T. M. Altahtamouni,** (2019). A brief overview of RF sputtering deposition of boron carbon nitride (BCN) thin films, *Emergent Materials*, 2(1), 79–93.

[97] "Handbook of Sputter Deposition Technology."

[98] **M. Ohring,** *Materials Science of Thin Films Second Edition*.

[99] **E. Avendaño, A. Azens, J. Isidorsson, R. Karmhag, G. A. Niklasson, and C. G. Granqvist,** (2003). Optimized nickel-oxide-based electrochromic thin films, Solid State Ionics, 165(1-4), 169-173, 2003.

[100] **P. S. Nnamchi and C. S. Obayi,** (2018). *Electrochemical characterization of nanomaterials*. Elsevier Ltd..

[101] **B. E. Yoldas and D. P. Partlow,** (1985). FORMATION OF BROAD BAND ANTIREFLECTIVE COATINGS FUSED SILICA FOR HIGH POWER LASER APPLICATIONS ON, 129, 1985.

[102] **D. S. Dalavi *et al.*,** (2011). Nanoporous nickel oxide thin films and its improved electrochromic performance: Effect of thickness," *Applied Surface Science*, 257(7), 2647–2656.

[103] **P. Salunkhe, A. V. Muhammed Ali, and D. Kekuda,** (2020). Investigation on tailoring physical properties of Nickel Oxide thin films grown by dc magnetron sputtering, *Materials Research Express*, 7, 1.

[104] **S. Passerini,** (1990). The Intercalation of Lithium in Nickel Oxide and Its Electrochromic Properties, *Journal of The Electrochemical Society*, 137(10), 3297.

[105] **Y. Sen Lin *et al.*,** (2010). Electrochromic performance of reactive plasma-sputtered NiOx thin films on flexible PET/ITO substrates for flexible electrochromic devices, *Surface and Coatings Technology*, 205, 1, S216–S221.

[106] **Q. Liu *et al.*,** (2018). In situ electrochromic efficiency of a nickel oxide thin film: Origin of electrochemical process and electrochromic degradation,*Journal of Materials Chemistry C*, 6, (3), 646–653.

[107] **A. I. Inamdar *et al.*,** (2011). Electrochromic and electrochemical properties of amorphous porous nickel hydroxide thin films, *Applied Surface Science*, 257(22), 9606-9611.

[108] **Y. Zhao *et al.*,** (2018). Sputtering power induced physical property variation of nickel oxide films by radio frequency magnetron sputtering, *Materials Research*, 21(2), 7–10.

CURRRICULUM VITAE

Name Surname **:** Ece KURT

EDUCATION

- **B.Sc.** **:** 2017, Hacettepe University, Faculty of Engineering, Physics Engineering
- **M.Sc.** **:** 2021, Istanbul Technical University, Department of Physics Engineering, Physics Engineering

PROFESSIONAL EXPERIENCE

- **Long Term Internship in ŞİŞECAM Science Technology and Design Center,** Electrochromic device design, deposition, and characterization. (01.2018-11.2018)
- **Junior Researcher at Şişecam Science Technology and Design Center** (2021-)

PRESENTATION

- Science and Applications of Thin Films, Conference & Exhibition (SATF 2018), The Effect of Sputtering Power and Oxygen Partial Pressure on the Electrochromic Properties of NiO Grown by Magnetron Sputtering (presentation)
- Sisecam 33. Cam Sempozyumu Yapay Zeka ve Cam Sektörü (2018), Ece Kurt, Öcal Tuna, Duygu Kalkan, Melih Üstün, Lukas Simurka, S. Türküz, "Magnetron Sıçratma Kaplama Gücü ve Oksijen Kısmi Basıncının Nikel Oksit İnce Filmlerin Elektrokromik Özelliklerine Etkisi" (presentation).

PUBLICATION

- **Feresteh Ordokhani, Beyza Yedikardeş, Ece Kurt, Nihat Akkan, Nilgün Karatepe, Esra Zayim, Mustafa Altun**, (2021) Improving Threshold Voltage

and on/off current ratio of Single-Walled Carbon Nanotube Field-Effect Transistor by Post-Sonication Treatments, Thin Solid Films (https://doi.org/10.1016/j.tsf.2021.138677)

- **Beyza Yedikardeş, Feresteh Ordokhani, Ece Kurt, Nihat Akkan, Nilgün Karatepe Yavuz, Esra Zayim, Mustafa Altun**, (2021) Enhanced Electrical Properties of P3HT:WO3 Hybrid Thin Film Transistors (https://doi.org/10.1016/j.tsf.2021.138677)